Review

Robert Schönherr, Janine Mia Rudolph and Lars Redecke*

Protein crystallization in living cells

https://doi.org/10.1515/hsz-2018-0158
Received February 12, 2018; accepted May 7, 2018

Abstract: Protein crystallization in living cells has been observed surprisingly often as a native assembly process during the past decades, and emerging evidence indicates that this phenomenon is also accessible for recombinant proteins. But only recently the advent of high-brilliance synchrotron sources, X-ray free-electron lasers, and improved serial data collection strategies has allowed the use of these micrometer-sized crystals for structural biology. Thus, *in cellulo* crystallization could offer exciting new possibilities for proteins that do not crystallize applying conventional approaches. In this review, we comprehensively summarize the current knowledge of intracellular protein crystallization. This includes an overview of the cellular functions, the physical properties, and, if known, the mode of regulation of native *in cellulo* crystal formation, complemented with a discussion of the reported crystallization events of recombinant proteins and the current method developments to successfully collect X-ray diffraction data from *in cellulo* crystals. Although the intracellular protein self-assembly mechanisms are still poorly understood, regulatory differences between native *in cellulo* crystallization linked to a specific function and accidently crystallizing proteins, either disease associated or recombinantly introduced, become evident. These insights are important to systematically exploit living cells as protein crystallization chambers in the future.

***Corresponding author: Lars Redecke,** Institute of Biochemistry, Center for Structural and Cell Biology in Medicine, University of Lübeck, Ratzeburger Allee 160, D-23562 Lübeck, Germany; and Deutsches Elektronen Synchrotron (DESY), Notkestrasse 85, D-22607 Hamburg, Germany,
e-mail: redecke@biochem.uni-luebeck.de
Robert Schönherr: Institute of Biochemistry, Center for Structural and Cell Biology in Medicine, University of Lübeck, Ratzeburger Allee 160, D-23562 Lübeck, Germany; and Deutsches Elektronen Synchrotron (DESY), Notkestrasse 85, D-22607 Hamburg, Germany
Janine Mia Rudolph: Institute of Biochemistry, Center for Structural and Cell Biology in Medicine, University of Lübeck, Ratzeburger Allee 160, D-23562 Lübeck, Germany; and Center for Free-Electron Laser Science (CFEL), DESY, Notkestrasse 85, D-22607 Hamburg, Germany

Keywords: *in cellulo* crystallization; *in vivo* crystals; microcrystallography; protein crystallography; serial crystallography; X-ray free-electron laser.

Introduction

The crystalline state of biological macromolecules is the prerequisite for X-ray crystallography, a powerful method for obtaining structural information of proteins at atomic resolution. In traditional synchrotron X-ray crystallography, the inherent correlation between crystal size and diffraction intensity usually requires the growth of sufficiently large and homogeneous single crystals, combined with cryogenic conditions during data collection to reduce radiation damage (Holton and Frankel, 2010). Diverse strategies to crystallize recombinant proteins in artificial chambers have been established within the past decades (Chayen and Saridakis, 2008), but there is still no guarantee for crystal formation, particularly for post-translationally modified proteins and membrane proteins (Bill et al., 2011).

The challenges in crystal growth might reflect a negative evolutionary pressure that prevents spontaneous intracellular protein crystallization, as aggregation frequently compromises the native protein function and thus the viability of the cell (Doye et al., 2004). Consequently, crystal formation within living cells was largely considered as an atypical event, although known for more than a century. The first reports date back to the 1850s, when protein crystals in human tissue and in the seeds of the Brazil nut were initially described (Charcot and Robin, 1853; Hartig, 1855), followed by several other examples to date. These observations strongly indicate that protein crystallization represents a native, if somewhat rare process that provides defined advantageous functions for the organism, mainly associated with storage, protection and solid state catalysis. On the other hand, the abnormal crystalline state of proteins that are usually soluble within the cell was identified as a characteristic pathogenic hallmark, as observed for certain forms of human cataracts and anemia (Pande et al., 2001; Vekilov et al., 2002).

In cellulo crystallization of recombinant proteins during gene expression represents another form of

abnormal protein assembly. Although initially reported in 1996 (Fan et al., 1996), it took 14 years until two additional examples were detected (Brandariz-Nuñez et al., 2010; Hasegawa et al., 2011). The crowded environment in the living cell was supposed to prevent the growth of sufficiently ordered crystals. Moreover, due to the small size, which was assumed to be necessarily limited by the cell's outer dimensions (Doye and Poon, 2006), *in cellulo* crystals harbor only low diffraction capabilities, particularly for X-rays produced by the available synchrotron sources at that time. Thus, *in cellulo* crystals were not considered for structural biology for many years, preventing a systematic investigation of this phenomenon. The situation significantly changed within the past decade, mainly driven by the commissioning of microfocus beamlines (Yamamoto et al., 2017) and X-ray free-electron lasers that produce radiation of previously inaccessible energy and brilliance (Yabashi and Tanaka, 2017), but also by the development of novel serial data collection strategies (Chapman et al., 2011). In 2007, the first structure of a natively crystallizing protein, cypoviral polyhedrin, was reported (Coulibaly et al., 2007), followed in 2012 by the important proof that intracellular crystals formed by a recombinant, not naturally crystallizing protein can be used to extract high-resolution structural information (Redecke et al., 2013).

Driven by this success, a significant number of protein microcrystals has nowadays been discovered in living cells. As structural information of the associated proteins was elucidated several fold (Table 1), it is now accepted that *in cellulo* grown crystals are indeed suitable targets for structural biology. However, it is still not clear whether or not the phenomenon of *in cellulo* crystallization is restricted to a limited number of proteins that are evolutionary optimized for native crystal formation to provide a specific function, complemented by only a few accidental crystallization events. A comprehensive look at this fascinating phenomenon is crucial to identify elements and strategies as "common" features for both native and accidental *in cellulo* protein crystallization, but also to highlight differences. A more detailed understanding of the associated cellular processes is required to systematically exploit living cells as crystallization chambers, which could offer exciting new possibilities for proteins that do not crystallize applying conventional approaches.

Native *in cellulo* crystallization

During the past century several native proteins have been described to crystallize in living cells. The majority were detected based on their regular morphology and dense packing, without knowledge of the identity and function of the assembled protein. These crystals occur in cells of all kingdoms of life without preference for a specific cellular compartment (Strunk, 1959; Freddo et al., 1980; Veenhuis et al., 1981; Hawkes, 1993; Vayssié et al., 2000; Nürnberger et al., 2017). Native crystal formation is usually associated with advantageous functions for the organism that exploit the specific properties of the crystalline state, as subsequently discussed and summarized in Table 2.

Protein storage

The dense packing of the crystalline lattice can provide a space-efficient way for permanent sequestration or temporary storage of functional proteins. Triggered by environmental changes, protein crystals dissolve, if required, resulting in high local concentrations of active protein. A frequent application of this strategy in nature is nutrient storage. In non-legume plant seeds membrane-surrounded storage organelles include 'crystalloids' consisting of an amorphous matrix with embedded protein packed in a lattice structure (Jiang et al., 2000), while oviparous animal species, e.g. *Drosophila melanogaster* (Papassideri et al., 2007), the mosquito *Aedes aegypti* (Snigirevskaya et al., 1997), but also frogs (Figure 1A) (Massover, 1971) or bony fish (Lange et al., 1982), crystallize yolk proteins in developing oocytes to provide a constant nutrient supply for the offspring. The viviparous cockroach *Diploptera punctata* follows a slightly different nourishment strategy. Crystals develop within the embryo midgut soon after ingestion of liquid milk (Figure 1B) (Ingram et al., 1977), a complex mixture of distinct lipocalin-like proteins secreted by the brood sac (Williford et al., 2004), providing a nutrient supply with 3 times the energy of an equivalent mass of dairy milk. Despite the remarkable protein heterogeneity within a single crystal the structural basis of the intracellular crystallizability of these milk proteins was recently elucidated at atomic resolution (Banerjee et al., 2016).

Virulence factors represent another important group of proteins that exploit the crystalline state for concentrated long-term storage in the environment, combined with protection from proteolytic degradation. Prominent examples include parasporal toxin crystals produced by ubiquitous Gram-positive spore-forming bacteria, e.g. *Bacillus thuringiensis* (Bt, Figure 1E) (Sawaya et al., 2014) and *Lysinibacillus sphaericus* (Colletier et al., 2016), or crystalline fusolin 'spindles' produced by insect poxviruses (Perera et al., 2010). Following ingestion by a susceptible insect, the so far stable crystals quickly dissolve in

Table 1: Overview of structurally investigated *in cellulo* crystals of natively crystallizing proteins as well as of *in cellulo* crystallizing recombinant proteins.

Name	Source organism	Host organism	Compartment	Morphology	Max crystal size	X-ray method	Resolution	PDB entry	Reference
Bt toxins	*B. thuringiensis* subsp. *aizawai* IPL7	*E. coli* JM103	None	Dipyramidal	n/d	None used	n/a	n/a	(Oeda et al., 1989)
Calcineurin (CNA-CNB complex)	*N. crassa* (CNA/NorfA), *H. sapiens* (CNB)	Insect cells (Sf21, Sf9, HighFive)	Cytoplasm	Cubic, pyramidal	$10\times6\times6\ \mu m^3$	None used	n/a	n/a	(Fan et al., 1996)
Pea legumin A	Pea	*T. aestivum* (transgenic wheat)	Vacuole	Rhomboidal	$3\times3\times3\ \mu m^3$	None used	n/a	n/a	(Stöger et al., 2001)
Cry2Aa2	*B. thuringiensis*	Tobacco plant	Chloroplast	Cuboidal	n/d	None used	n/a	n/a	(De Cosa et al., 2001)
Polyhedrin	*B. mori* CPV1	Insect cells	Cytoplasm	Cubic, body-centered	$2\times2\times2\ \mu m^3$	MSX, >300 isol. crystals, 100 K, MicroMeshes	1.98 Å	2OH5, 2OH6, 2OH7	(Coulibaly et al., 2007)
Polyhedrin	G25D AcMNPV	Insect cells (Sf21)	Cytoplasm, nucleus	Cubic, body-centered	$15\times15\times15\ \mu m^3$	MSX, 17 isol. crystals, 100 K, MicroMeshes	2.3 Å	3JW6	(Coulibaly et al., 2009)
Polyhedrin	*Wisena* NPV	Porina larvae, *W. spp*	Cytoplasm	Cubic, body-centered	$4\times4\times4\ \mu m^3$	MSX, 19 isol. crystals, 100 K, MicroMeshes	2.18 Å	3JVB	(Coulibaly et al., 2009)
Green fluorescent protein-μNS fusion protein	*A. victoria*/Reovirus	Primary cultures of chicken embryo fibroblast (CEFs), insect cells (Sf9)	Cytoplasm	Needles, hexagonal base	$3\times3\times10\ \mu m^3$	None used	n/a	n/a	(Brandariz-Nuñez et al., 2010)
Polyhedrin	G25D AcMNPV	Insect cells (Sf9)	Cytoplasm, nucleus	Cubic, body-centered	$15\times15\times15\ \mu m^3$	MSX, 17 isol. crystals, 100 K, MicroMeshes	1.84 Å	2WUX	(Ji et al., 2010)
Polyhedrin	AcMNPV	Insect cells (Sf9)	Cytoplasm, nucleus	Cubic, body-centered	$5\times5\times5\ \mu m^3$	MSX, 7 isol. crystals, 100 K, MicroMeshes	3.09 Å	2WUY	(Ji et al., 2010)
Human immunoglobulin G2	*H. sapiens*	Mammalian cells (CHO)	ER	Needles	$5\times5\times50\ \mu m^3$	None used	n/a	n/a	(Hasegawa et al., 2011)
Cathepsin B	*T. brucei*	Insect cells (Sf9)	ER	Needles, square base	$2\times2\times30\ \mu m^3$	SFX, 178875 isol. crystals, RT, liquid jet	2.1 Å	4HWY	(Redecke et al., 2013)
Inosine monophosphate dehydrogenase	*T. brucei*	Insect cells (Sf9)	Cytoplasm, peroxisomes	Needles, square base	$4\times4\times60\ \mu m^3$	None used	n/a	n/a	(Nass, 2013)
Polyhedrin	*O. brumata* CPV18	Insect cells (Sf9)	Cytoplasm	Cubic, body-centered	$4.5\times4.5\times4.5\ \mu m^3$	*In cellulo* MSX, 20 crystals, 100 K, MicroMeshes	1.7 Å	4OTV	(Axford et al., 2014)
Polyhedrin	*O. brumata* CPV18	Insect cells	Cytoplasm	Cubic, body-centered	$5\times5\times5\ \mu m^3$	MSX, 20 isol. crystals, 100 K, MicroMeshes	1.7 Å	4OTS	(Axford et al., 2014)
Cathepsin B	*T. brucei*	Insect cells (Sf9)	ER	Needles, square base	$2\times2\times30\ \mu m^3$	SSX, 80 isol. crystals, 100 K, loop	3.0 Å	4N4Z	(Gati et al., 2014)
Cry3A	*B. thuringiensis* subsp. *morrisoni*, strain *tenebrionis*	*B. thuringiensis* subsp. *israelensis*, strain 4Q7	None	Rectangular platelets	$1.5\times1\times0.5\ \mu m^3$	*In cellulo* SFX, 736360 frames, RT, liquid jet	2.9 Å	4QX2, 4QX3	(Sawaya et al., 2014)

Table 1 (continued)

Name	Source organism	Host organism	Compartment	Morphology	Max crystal size	X-ray method	Resolution	PDB entry	Reference
Cry3A	*B. thuringiensis* subsp. *Morrisoni*, strain *tenebrionis*	*B. thuringiensis* subsp. *Israelensis*, strain 4Q7	None	Rectangular platelets	$1.5\times1\times0.5\ \mu m^3$	SFX, isol. crystals, 380688 frames, RT, liquid jet	2.8 Å	4QX0, 4QX1	(Sawaya et al., 2014)
Human immunoglobulin G2/λ; IgG1/λ	*H. sapiens*	HEK293 cells upon Brefeldin A treatment	Cytoplasm	Spindles; needles	$3\times3\times20\ \mu m^3$; $1\times1\times70\ \mu m^3$	None used	n/a	n/a	(Hasegawa et al., 2014)
Human immunoglobulin G2/λ; IgG1/λ, IgG4/λ	*H. sapiens*	Mammalian cells (CHO)	ER	Spindles; needles	$3\times3\times20\ \mu m^3$; $1\times1\times75\ \mu m^3$	None used	n/a	n/a	(Hasegawa et al., 2014)
Neuraminidase	*H. sapiens*	Mammalian cells (CHO, HEK293)	n/a	Cuboidal	$15\times15\times3\ \mu m^3$	SFX, isol. crystals, liquid jet	3 Å	n/a	(Gallat et al., 2014)
Neuraminidase	*H. sapiens*	Mammalian cells (CHO, HEK293)	n/a	Needles	$2\times2\times20\ \mu m^3$	None used	n/a	n/a	(Gallat et al., 2014)
Polyhedrin	*O. brumata* CPV18	Insect cells	Cytoplasm	Cubic, body-centered	$5\times5\times5\ \mu m^3$	MSX, 21 isol. crystals, 100 K, MicroMeshes	1.48 Å	5A9P	(Ji et al., 2015)
Polyhedrin	*A. mylitta* CPV4	Insect cells (Sf9)	Cytoplasm	Cubic, body-centered	$7\times7\times7\ \mu m^3$	MSX, 18 isol. crystals, 100 K, MicroMeshes	1.72 Å	5A8S, 5A8T, 5A9C	(Ji et al., 2015)
Polyhedrin	*O. pseudotsugata* CPV5	Insect cells (Sf9)	Cytoplasm	Cubic, body-centered	$4\times4\times4\ \mu m^3$	MSX, 26 isol. crystals, 100 K, MicroMeshes	1.61 Å	5A8U, 5A8V	(Ji et al., 2015)
Polyhedrin	*L. dispar* CPV14	Insect cells (Sf9)	Cytoplasm	Cubic, body-centered	$4\times4\times4\ \mu m^3$	MSX, 20 isol. crystals, 100 K, MicroMeshes	1.91 Å	5A96	(Ji et al., 2015)
Polyhedrin	*T. ni* CPV15	*T. ni*	Cytoplasm	Cubic, body-centered	$1.5\times1.5\times0.5\ \mu m^3$	MSX, 40 isol. crystals, 100 K, MicroMeshes	1.82 Å	5A98	(Ji et al., 2015)
Polyhedrin	*U. sapphirina* CPV17	*U. sapphirina*	Cytoplasm	Cubic, body-centered	$1\times1\times1\ \mu m^3$	SFX, 5787 isol. crystals, RT, liquid jet	1.75 Å	4S1K	(Ginn et al., 2015; Ji et al., 2015)
Polyhedrin	*U. sapphirina* CPV17	*U. sapphirina*	Cytoplasm	Cubic, body-centered	$1\times1\times1\ \mu m^3$	MSX, 768 isol. crystals, 100 K, MicroMeshes	2.2 Å	4S1L	(Ginn et al., 2015; Ji et al., 2015)
Polyhedrin	*O. brumata* CPV19	Insect cells (Sf9)	Cytoplasm	Cubic, body-centered	$3\times3\times3\ \mu m^3$	MSX, 34 isol. crystals, 100 K, MicroMeshes	1.51 Å	5A99	(Ji et al., 2015)
Polyhedrin	*S. ubiquitum* CPV20	Insect cells (Sf9)	Cytoplasm	Cubic, body-centered	$4\times4\times4\ \mu m^3$	MSX, 51 isol. crystals, 100 K, MicroMeshes	1.82 Å	5A9A	(Ji et al., 2015)
Polyhedrin	*B. mori* CPV1	Insect cells	Cytoplasm	Cubic, body-centered	$2\times2\times2\ \mu m^3$	MSX, 13 isol. crystals, 100 K, MicroMeshes	1.88 Å	5A9B	(Ji et al., 2015)
Fusolin	Entomopoxvirus	Infected insects, e.g *M. melolontha*	ER	Bipyramidal	$8.5\times3.5\times3.5\ \mu m^3$	MSX, 100 K, MicroMeshes	1.9 Å	4YN1	(Chiu et al., 2015)
Green fluorescent protein-μNS fusion protein	*A. victoria*/Reovirus	Insect cells (Sf9)	Cytoplasm	Needles, hexagonal base	$5\times5\times15\ \mu m^3$	Powder, isolated crystals	30 Å	n/a	(Schönherr et al., 2015)

Table 1 (continued)

Name	Source organism	Host organism	Compartment	Morphology	Max crystal size	X-ray method	Resolution	PDB entry	Reference
Luciferase	*P. pyralis*	Insect cells (Sf9)	Cytoplasm, peroxisomes	Needles, square base	$2\times2\times200\ \mu m^3$	None used	n/a	n/a	(Schönherr et al., 2015)
Xpa	Engineered from *F. favus*	Mammalian cells (HEK293)	Cytoplasm, nucleus	Rhomboid	$4\times4\times7\ \mu m^3$	*In cellulo* SXD, 100 K	2.9 Å	4P76	(Tsutsui et al., 2015)
Xpa	Engineered from *F. favus*	Mammalian cells (hippocampal neurons)	Cytoplasm	Needle	$3\times3\times20\ \mu m^3$	None used	n/a	n/a	(Tsutsui et al., 2015)
PAK4-Inka1 complex	*H. sapiens*	Mammalian cells (HEK293, HeLa S3, COS-7)	Cytoplasm	Needles, hexagonal base	$5\times5\times100\ \mu m^3$	MSX, 5 *in cellulo* crystals	2.94 Å	4XBR	(Baskaran et al., 2015)
Eosinophil major basic protein	*H. sapiens*	–	Exosomes	Needles	$0.5\times0.5\times0.5\ \mu m^3$	SFX, crystals in isolated granules (from blood), fixed target	ca. 4 Å	n/a	(Soragni et al., 2015)
BinAB	*L. sphaericus*	*B. thuringiensis*	None	Polygonal	$0.5\times0.4\times0.4\ \mu m^3$	SFX, MIRAS, both with isolated nanocrystals	2.25 Å	5FOY, 5FOZ, 5G37	(Colletier et al., 2016)
Polyhedrin	*B. mori* CPV1	Insect cells	Cytoplasm	Cubic, body-centered	$2\times2\times2\ \mu m^3$	MSX, 9 *in cellulo* crystals, 100 K, MicroMeshes	1.55 Å	5EXY,	(Boudes et al., 2016)
Polyhedrin	*B. mori* CPV1	Insect cells	Cytoplasm	Cubic, body-centered	$2\times2\times2\ \mu m^3$	MSX, 7 isol. crystals, 100 K, MicroMeshes	1.9 Å	5EXZ	(Boudes et al., 2016)
Methanol oxidase	*H. polymorpha*	–	Peroxisome	Cubic	$1\times1\times1\ \mu m^3$	SFX, fixed cells, RT, liquid jet	5.6 Å	n/a	(Jakobi et al., 2016)
Lili-Mip	*D. punctata*	–	None	Cuboidal	$10\times10\times30\ \mu m^3$	SXD, isol., 100 K	1.2 Å	4NYQ	(Banerjee et al., 2016)
Polyhedrin	*O. brumata* CPV18	Insect cells	Cytoplasm	Cubic, body-centered	$4\times4\times4\ \mu m^3$	SFX, 100 K, fixed target high-speed goniometer	2.4 Å	5MQV	(Roedig et al., 2017)
Granulin	Granulovirus	*P. interpunctella*	Cytoplasm	Ovocylindrical angular or hexagonal	$0.4\times0.2\times0.2\ \mu m^3$	SFX, isol. granulovirus OBs, liquid jet, gas-focused nozzle	1.66 Å	5G0Z	(Gati et al., 2017)
Granulin	Granulovirus	*P. interpunctella*	Cytoplasm	Ovocylindrical angular or hexagonal	$0.4\times0.2\times0.2\ \mu m^3$	SFX, isolated granulovirus OBs, liquid jet, double flow-focusing nozzle	2.56 Å	5MND	(Oberthuer et al., 2017)

isol., Isolated crystals; MIRAS, multiple isomorphous replacement with anomalous scattering; MSX, multiple-crystal synchrotron crystallography; OB, occlusion body; SFX, serial femtosecond crystallography; SSX, serial synchrotron crystallography; SXD, single-crystal X-ray diffraction applying synchrotron radiation.

Table 2: Natively crystallizing proteins in living cells that have not been used for structural studies, ordered according to their function.

Function	Protein	Description	Source organism	Compartment	Morphology	Detection method	Reference
Storage	Tobacco seed protein	Seed protein isolated from tobacco plant seeds	Tobacco plant	n/d	Isotropic octahedra	Powder diffraction	(Crowfoot and Fankuchen, 1938)
	Edestin	Seed protein from hemp seeds	Hemp plant	n/d	n/d	TEM	(Hall, 1950)
	Vitellin	Yolk protein crystallizing in mitochondrion cristae	Bullfrog oocytes	Mitochondria (intermembrane space)	Needle with hexagonal base	TEM	(Massover, 1971)
	Vitellin	Yolk protein crystallizing in mitochondrion cristae	Leopard frog	Mitochondria (intermembrane space)	Needle with hexagonal base	TEM	(Ward, 1962)
	Insulin	Peptide hormone in pancreatic islets	*H. sapiens*	Exosomes	Needles with hexagonal or rhombohedral base	TEM	(Raška et al., 1978)
	Cucurbitin	Crystalline storage vesicle	Rock Melon	n/d	n/d	TEM	(Colman et al., 1980)
	Lipovitellin-phosvitin	Yolk protein crystals	Bony Fish oocytes	n/d	n/d	TEM	(Lange et al., 1982)
	Vitellin	Yolk protein crystals	*A. aegypti* oocytes	Yolk bodies	Rounded crystalline structures	Immuno-labeling EM	(Snigirevskaya et al., 1997)
	Trichocyst matrix proteins	Molecular spring through crystal expansion	*Paramecium*	Exosomes	Rod-shaped or needles	TEM	(Vayssié et al., 2000)
	Cry proteins	Parasporal proteinaceous crystals	*B. thuringiensis*	None	Bipyramidal or platelets	TEM	(Evdokimov et al., 2014; Sawaya et al., 2014)
Encapsulation	Spheroidin	Capsule of entomopoxvirus	*B. mori*	n/d	Spherical	TEM	(Takemoto et al., 2008)
	S-layer proteins	Bacterial surface layers covering archaea and some bacteria	Various archaea and bacteria	Extracellular	2D lattice carpet	TEM	(Sleytr et al., 2014)
	Dps + DNA	'Biocrystals' protecting bacterial DNA	*E. coli*	None	Irregular crystalline cores	TEM	(Wolf et al., 1999)
Compartmentalization	Metabolosomes	Intracellular polyhedral bodies in various bacteria	e.g. *T. neapolitanus*	None	Polygonal	TEM	(Shively et al., 1973)
Solid state catalysts	Urate oxidase		*R. norvegicus* (Wistar)	Peroxisomes	Irregular crystalline cores	TEM	(Tsukada et al., 1966)
	Alcohol oxidase		*H. polymorpha*	Peroxisomes	Cubes	TEM	(Vonck and van Bruggen, 1992)
	Catalase		Sunflower (*H. annuus L.*)	Peroxisomes	Cubes	HRSEM	(Heinze et al., 2000)
Wound sealing	Hex-1	Fungal crystals to seal the septal core	*N. crassa* (and other ascomycetes)	Woronin bodies/ peroxisomes	Hexagonal	TEM	(Markham and Collinge, 1987; Yuan et al., 2003)
	P-protein	Seal for the phloem sieve tube in plants	*V. faba*	Cytoplasm	Spindle	EM, confocal laser scanning microscopy	(Knoblauch et al., 2001; van Bel, 2003)

Table 2 (continued)

Function	Protein	Description	Source organism	Compartment	Morphology	Detection method	Reference
Disease associated crystals	CLC protein/ galectin-10	Charcot-Leyden crystals	*H. sapiens*	Exosomes	Hexagonal bipyramidal	LM	(Weller et al., 1984)
	Mitochondrial creatine kinase	Mitochondrial crystalline inclusions	*H. sapiens*	Mitochondria	Cubic/needles	TEM	(Farrants et al., 1988)
	Hemoglobin C	Hemoglobin C disease	*H. sapiens*	Cytoplasm	Hexagonal rods	SEM, LM	(Lawrence et al., 1991)
	Gamma-D crystallin	Cataract	*H. sapiens*	Cytoplasm	Needles	Transillumination slit-lamp	(Héon et al., 1999)
	Unknown protein	Reinke crystals	*H. sapiens*	Cytoplasm, nucleus	Rod-like hexagonal	Histologic stains, LM	(Kozina et al., 2011)
Unknown function	Unknown protein	Iron containing protein in midgut glands; possibly a secretory protein	*L. lignorum*	Golgi complex	Self-assembling stacks forming bipyramidal crystals	TEM, Prussian blue reaction for iron	(Strunk, 1959)
	Unknown protein	Crystals in equine chondrocytes	Horse – Haflinger	Mitochondria	Needles	TEM, histologic stains	(Nürnberger et al., 2017)

The characterization includes crystal compartment and – morphology, in addition to the original detection method. EM, electron microscopy; HRSEM, high resolution scanning electron microscopy; LM, light microscopy; SEM, scanning electron microscopy; TEM, transmission electron microscopy.

the alkaline gut. The release of the active proteins induces a multi-step intoxication process that finally allows bacterial endospores to germinate in the insect hemolymph (Sanahuja et al., 2011) or disrupts the chitin-rich peritrophic matrix of the insect to facilitate the oral poxyvirus infection (Chiu et al., 2015). As the unique activity of these microbial bioinsecticides (Schnepf et al., 1998) is usually combined with a narrow taxonomic specificity, safety for mammals, and biodegradability, virulence factors are of significant commercial interest in agriculture (Sanahuja et al., 2011). Nowadays, high-resolution structures are available from *in cellulo* grown crystals of poxivirus fusolin (Chiu et al., 2015), of the Bt Cry3A toxin (Sawaya et al., 2014), and of the binary *L. sphaericus* toxin BinAB (Colletier et al., 2016), complemented by structural information of the toxic core domains from various mature Bt toxins that were usually obtained after re-crystallization of dissolved native microcrystals (Schnepf et al., 1998; Adalat et al., 2017). However, there is evidence for the function of the associated protoxin state as an enhancer of native crystal packing and stability, provided by the first full-length protoxin structure that was recently elucidated (Evdokimov et al., 2014).

Proteins involved in regulated secretory pathways are frequently stored in a highly condensed amorphous or crystalline state in granules, ready for exocytotic release in response to an external trigger (Arvan and Castle, 1998). The most prominent and best understood example represents insulin, which has been comprehensively reviewed in terms of structure, function and regulated crystallization (Dodson and Steiner, 1998). In eosinophils, the tightly controlled crystalline self-association of a granular protein acts as a regulatory switch (Frigas and Gleich, 1986). Participating in the innate immune response against bacteria and viruses, these cells secrete highly cytotoxic proteins from their granules, e.g. the eosinophil major basic protein (MBP-1) that disrupts the membranes of pathogens (Giembycz and Lindsay, 1999). Safe intra-granular storage in host cells is only enabled by packing MBP-1 into crystalline structures (Figure 1C) that restrain toxicity, which have recently been used for diffraction tests applying SFX techniques (Soragni et al., 2015). Moreover, crystalline secretory granules can trigger a remarkable physical impulse that pushes a cell away from a potential predator, as observed for *Paramecium* cells belonging to the mainly unicellular eukaryotic protists (Vayssié et al., 2000). Triggered by calcium ion release, the concerted exocytosis of more than 1000 secretory granules docked at the plasma membrane rapidly propels the cells in the opposite direction. The driving force is a roughly seven-fold expansion of the crystalline

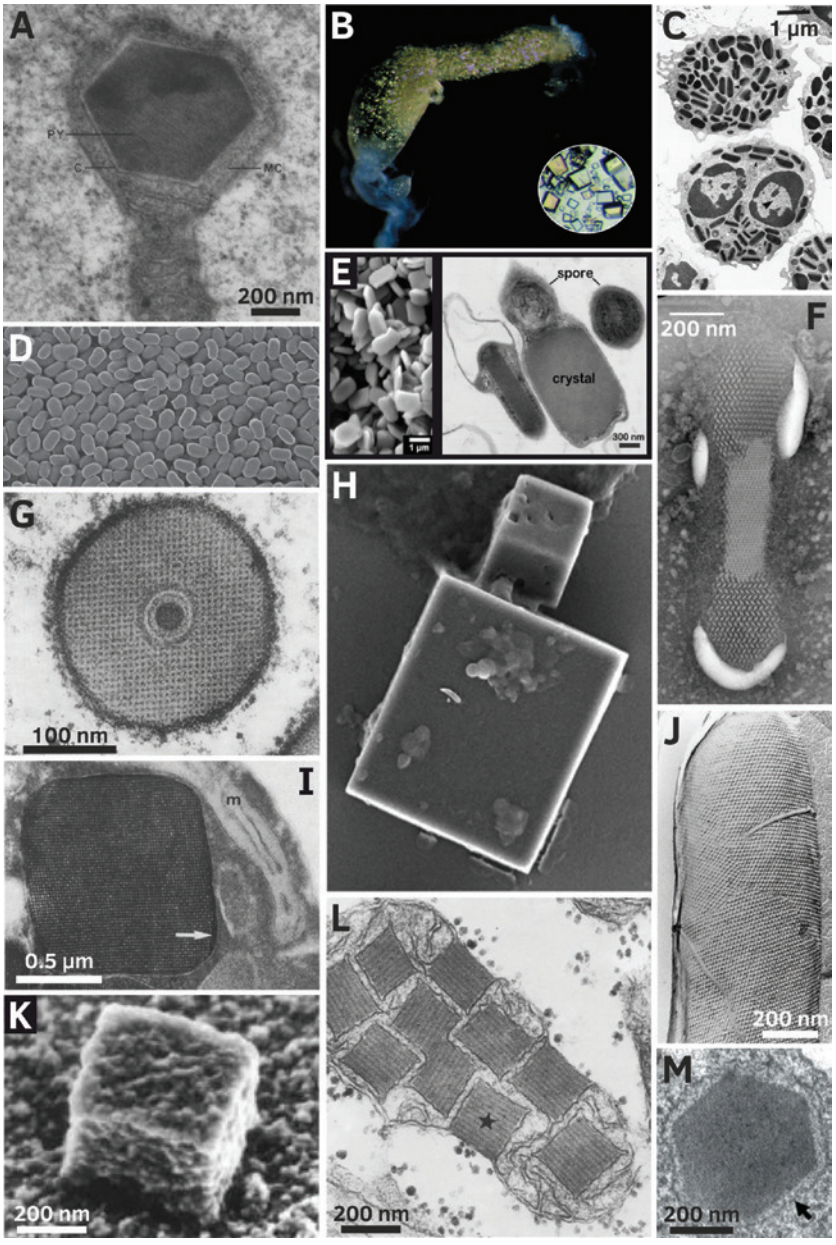

Figure 1: Examples of naturally occurring protein crystals.
(A) A hexagonal crystal embedded in the mitochondrial cortex of a *Rana pipiens* oocyte that develops yolk platelet crystals (Republished with permission of Rockefeller University Press from Ward (1962); permission conveyed through Copyright Clearance Center, Inc.). (B) *In vivo*-grown Lili-Mip crystals from *D. punctata* enclosed inside the embryo midgut (Banerjee et al., 2016; reproduced with permission of the International Union of Crystallography). (C) MBP-1 crystals enclosed in vesicles in untreated eosinophils, purified from the peritoneal cavity of guinea pigs (Giembycz and Lindsay, 1999). (D) Granulovirus (CpGV) occlusion bodies purified from infected larvae of *C. pomonella* (Gati et al., 2017). (E) Rectangular platelet crystals of the Cry3A toxin from *B. thuringiensis* subsp. *morrisoni* expressed in *Bt* subsp. *israelensis*, within intact bacterial cells (right panel) and after isolation (left panel) (Sawaya et al., 2014). (F) A secretory granule of *Tetrahymena thermophile*, in which the crystalline core has started to expand at both ends of the granule (Turkewitz, 2004; reproduced with permission of John Wiley and Sons). (G) Transverse section through a granulovirus rod in its capsule within an infected larva of *Plodia interpunctella* (Reprinted from Arnott and Smith (1967) with permission from Elsevier). (H) Isolated baculoviral polyhedra from G25D AcMNPV (Coulibaly et al., 2009). (I) Crystalline alcohol oxidase in peroxisomes in methanol-grown cells of the yeast *Hansenula polymorpha* (Reprinted by permission from Springer Nature: Veenhuis et al., 1978). (J) Crystalline S-layer coat covering a bacterial cell (Sára and Sleytr, 2000; reproduced with permission from American Society for Microbiology). (K) Catalase-containing crystalline peroxisomal core from 5-days-old sunflower cotyledons (Heinze et al., 2000; reproduced with permission of John Wiley and Sons). (L) Paracrystalline mitochondrial inclusions in normal human skeletal muscle (Reprinted by permission from Springer Nature: Hammersen et al., 1980). (M) Hex-1 crystal in a Woronin body from *Neurospora crassa* (Reprinted by permission from Springer Nature: Yuan et al., 2003).

cargo of the granules (Figure 1F) that is expelled as needle-like structures (Turkewitz, 2004).

Protection and stabilization

Many viruses form paracrystalline arrays in infected host cells that contribute to the ordered intracellular virion assembly, mainly by providing a stable matrix for the spatial arrangement. Although well-analyzed by EM, recent investigations applying SFX and cryo-electron tomography improved the structural insights into these arrays (Duyvesteyn et al., 2018; Ke et al., 2018). If the mechanical properties are further improved by extension of the intermolecular lattice interactions, the stability of a crystalline matrix can be exploited as a protection mechanism. This strategy is adopted by cytoplasmic (CPV) and nuclear polyhedrosis viruses (NPV), granulosis viruses, as well as entomopoxviruses, which encapsulate virions in the late stage of infection by a robust crystalline polyhedrin, granulin, or spheroidin coat, respectively, that survives harsh environmental conditions (Smith, 1976; Coulibaly et al., 2007). As the embedded virus particles remain stable and infectious in soil for many years until ingested by insect larvae, the crystalline state additionally provides an efficient delivery system between hosts by oral-fecal routes (Rohrmann, 1986). Only the specific alkaline target environment in the midgut quickly dissolves the crystalline coat and releases the infectious viral particles (Payne and Mertens, 1983).

Polyhedra produced by two completely unrelated insect viruses, baculoviruses (family *Baculoviridae*, NPV) and cypoviruses (family *Reoviridae*, CPV), represent the best investigated crystalline coat so far (Coulibaly et al., 2007, 2009; Ji et al., 2015). A well-ordered and densely packed polyhedrin lattice (Figure 1H) incorporates up to several thousands of uniformly distributed virus particles within holes (Hill et al., 1999). A comprehensive database currently consisting of three different NPV and nine different CPV polyhedrin high-resolution structures (Coulibaly et al., 2007, 2009; Ji et al., 2010, 2015; Axford et al., 2014; Ginn et al., 2015) illustrates that the overall polyhedra architecture is highly conserved during evolution, despite considerable different life cycles of baculo- and cypoviruses as well as significant variability in the sequences and individual three-dimensional (3D) structures of CPV and NPV polyhedrin (Coulibaly et al., 2007, 2009; Ji et al., 2010). A consistent overall architecture of the crystalline granulin coat that encapsulates the *Cydia pomonella* granulovirus (CpGV, Figure 1D and G) (Gati et al., 2017; Oberthuer et al., 2017), which is closely related to NPV, further supports a preference of the observed geometry for protection of enclosed virions (Anduleit et al., 2005; Ji et al., 2015).

Filamentous fungi and plants developed another strategy to exploit the stiffness and mechanical stability of a crystalline lattice. Here, protein crystals are used to seal pores after damage to the cell, preventing cytoplasmic bleeding (van Bel, 2003; Yuan et al., 2003). In *Neurospora crassa*, as in numerous ascomycetes species, the occluding function is performed by organelles named Woronin bodies that localize in the vicinity of the septal pore (Markham and Collinge, 1987). The major proteinaceous component, Hex-1, self-assembles after import to form a robust hexagonal crystalline core (Figure 1M) that is required to withstand the high intracellular turgor pressure during pore sealing (Tenney et al., 2000). In plants, a comparable sealing strategy is based on the spindle-shaped crystalloid P-protein (Knoblauch et al., 2001).

In prokaryotes, native crystalline structures are known to be involved in cell wall stabilization, compartmentalization, and DNA protection. Self-assembled two-dimensional (2D) para-crystalline protein lattices, named S-layers, form a porous coating of 5–10 nm thickness around bacteria (Figure 1J) that has been associated with various functions (Sleytr et al., 2014). In archaea, S-layers constitute the only cell wall component in most species, frequently assembling into much thicker structures (Albers and Meyer, 2011). Another function of crystalline 2D layers is to form 100–200 nm sized bacterial microcompartments, so-called metabolosomes, that provide a specialized reaction environment for catabolic functions (Kerfeld and Erbilgin, 2015). Confinement of sequential enzymatic reactions facilitates substrate channeling and protects the cell from potentially harmful reaction intermediates (Plegaria and Kerfeld, 2017). The third example exploits a native crystallization process to protect bacterial DNA against stress (Luijsterburg et al., 2006). During the stationary phase, the genomic DNA of *E. coli* forms, together with RNA and certain structural and regulatory proteins, a crystalline complex in the cytoplasm that contains the histone-like Dps (DNA-binding protein of starved cells) protein as the main component (Karas et al., 2015).

Solid state catalysts

Particularly in eukaryotic cells a few active enzymes are known to be natively organized in a crystalline state. Alcohol oxidase forms pure crystals within the peroxisomes of yeast cells fed on methanol (Figure 1I), but also heterogeneous compositions additionally containing

urate oxidase and glucose oxidase were observed, depending on the specific cell (Veenhuis et al., 2003). In higher plant peroxisomes, e.g. of the sunflower *Helianthus annuus L.*, catalase is crystallized in so-called 'cores' (Figure 1K) (Heinze et al., 2000), while urate oxidase seems to be the sole enzyme in nucleoids of rat liver cell microbodies (Tsukada et al., 1966). Although the reason for assembling active enzymes in a crystalline state is not clear, the crystal lattice might at least not be disadvantageous for the enzymes, as long as the active site is not blocked by crystal contacts. All relevant molecules are sufficiently small to reach the catalytic center by diffusion through channels in the crystal lattice and the specific translocation into peroxisomes diminishes the need for the enzymes to find their substrates by diffusion (Doye and Poon, 2006). Moreover, the confinement to protect the cell from potentially harmful reaction intermediates could spontaneously induce the self-assembly of the peroxisomal enzymes due to the high local concentrations.

Non-native *in cellulo* crystallization

If the crystallization process is tightly regulated, native *in cellulo* crystals can provide advantageous functions for the organism. However, small changes in the structure or in the environment of a usually soluble protein can also induce its accidental intracellular crystallization, which is historically recognized to be disease-associated. Moreover, there is increasing evidence that intracellular protein crystals develop as a consequence of recombinant gene expression in host cells, reflecting another type of abnormal crystallization process.

Disease-associated *in cellulo* crystals

If an abnormal crystalline state occurs in the cells of a patient suffering from a disease, it is often difficult to understand whether crystal formation represents the causative event of the disorder, a harmful side-effect, or a harmless byproduct (Doye and Poon, 2006), but at least two diseases are directly caused by abnormal protein crystallization. Congenital forms of cataract (Hejtmancik et al., 1995) are associated with mutations in genes encoding crystallins, the major components of the soluble lens proteins that maintain its transparency (Héon et al., 1999). Without affecting the overall protein fold, these mutations dramatically lower the protein solubility and support lattice formation, triggering the assembly of numerous prismatic crystals that result in lens opacification (Pande et al., 2001). Moreover, abnormal crystallization of a mutant hemoglobin form (HbC) in erythrocytes is known to cause a usually mild and chronic hemolytic anemia, denoted as hemoglobin C disease, which can be life-threatening for patients that are doubly heterozygous for both HbC and the sickle cell hemoglobin (HbS) (Nagel and Lawrence, 1991). The molecular basis of HbC diseases has extensively been studied (Vekilov et al., 2002; Chen et al., 2004; Feeling-Taylor et al., 2004).

For other examples, the impact of the intracellular crystalline state within the disease context is almost unknown. Hexagonal bipyramidal Charcot-Leyden crystals (CLCs) (Charcot and Robin, 1853; Leyden, 1872) assemble by auto-crystallization of galectin-10 in diverse human tissues, body fluids and secretions. If disease-related, the appearance of CLCs is considered as a hallmark of allergic, parasitic, neoplastic and inflammatory disorders (Ackerman et al., 2002). Crystal-storing histiocytosis (CSH) (Lewis et al., 2007) was associated with the accumulation of crystalline inclusions in the cytoplasm of histiocytes (Dogan et al., 2012), whereas rod-shaped hexagonal Reinke crystals are usually located within the cytoplasm of Leydig cells in the human testis (Reinke, 1896). Although the molecular nature of the crystals remains unclear (Kozina et al., 2011), the presence of Reinke crystals is pathognomonic for the identification of Leydig cell tumors and helpful in diagnosis (Jain et al., 2001). In a wide variety of neuromuscular diseases, e.g. in 'mitochondrial myopathies', cubic and needle shaped crystalline inclusions, which are suggested to consist of mitochondrial creatine kinase assembled by a so far unknown mechanism (Smeitink et al., 1992), represent a frequent feature in the mitochondrial intermembrane space of skeletal muscle fibers (Hurko et al., 1990). However, these inclusions also occur in healthy human tissue (Figure 1L) (Hammersen et al., 1980).

In cellulo crystallization of recombinant proteins

Different expression systems are well-established in laboratories to produce large quantities of recombinant proteins. The advantages and limitations of the individual systems have recently been discussed (Duszenko et al., 2015). As a consequence of recombinant gene expression, crystal growth within the host cells was already reported in plant cells, in chicken and mammalian cells, as well as in baculovirus-infected insect cells. In bacteria, only the crystallization of recombinant

insecticidal *B. thuringiensis* proteins (Figure 2H) is briefly mentioned (Oeda et al., 1989), while TEM analysis indicates the crystallization of the fungal protein HEX-1 in yeast cells (Würtz et al., 2008).

Plant cells

Legumin A, a major component of pea seed storage vacuoles, crystallizes when expressed in transgenic wheat endosperm during seed development (Stöger et al., 2001). Correlating with high legumin content angular crystals associated with inclusion bodies (Figure 2B) formed in the four outermost cell layers of the endosperm, subsequently extending into the vacuole. Moreover, the *B. thuringiensis* toxin Cry2Aa2 forms cuboidal crystals when expressed in tobacco plant chloroplasts (De Cosa et al., 2001).

Animal cells

In mammalian cells, crystalline states of four recombinant proteins are reported to date, supporting a more general qualification of this cellular environment to promote intracellular crystal growth. In CHO cells engineered for constitutive high-level expression of a human IgG clone, several needle-shaped crystals per cell (Figure 2D) grew within days in the ER lumen up to 50 μm length (Hasegawa et al., 2011). This was accompanied by cell enlargement and multi-nucleation, until the crystals extended the cell size, eventually disrupting the cell membrane. Comparable crystals were detected during transient human IgG expression in HEK293 cells, but only if cargo export from ER was blocked by chemical treatment. A genetically engineered coral fluorescent protein, denoted as Xpa, formed micron-sized crystals (Figure 2E) in transfected mammalian cells that were stable within the cell, but quickly dissolved after cell lysis (Tsutsui et al., 2015). While a needle-shaped morphology occurred in hippocampal neurons, one pyramidal crystal in the cytoplasm or in the nucleus was detected in 0.1% of transfected HEK293 cells, representing a comparatively low nucleation rate. The cytoplasmic crystals were enclosed in a membrane that indicates a lysosomal localization as a result of autophagic processes, which is more likely a response to the crystal formation than a trigger of nucleation. The autophagic machinery might selectively recognize the crystalline state after formation. In the case of degradation sensitive proteins, this in turn would require engineered mammalian cells with downregulated autophagy or impaired lysosomal activity to observe comparable *in cellulo* crystallization events (Tsutsui et al., 2015). Crystals of the metazoan-specific kinase PAK4 grew in the cytosol of a variety of transfected mammalian cell types (Figure 2F), but only in the presence of its potent endogenous inhibitor Inka1 (Baskaran et al., 2015). One needle-shaped crystal per cell with a maximum length of 100 μm was detected that exceeded the normal cell dimensions without disrupting the plasma membrane. The X-ray structure obtained by *in cellulo* crystal diffraction revealed a unique lattice that constitutes a hexagonal array of PAK4 subunits with channels of 80 Å in diameter running through the length of the crystal. Thus, the crystal might accommodate a variety of other proteins when fused to the kinase inhibitor, as initially demonstrated by Inka1-GFP, rating these crystals as a putative crystallization matrix that triggers the crystalline state of other protein 'cargos'.

Human neuraminidase forms a mixture of plate-shaped crystals with dimensions of up to $15\times15\times3$ μm^3 and needle shaped crystals with dimensions up to $2\times2\times20$ μm^3 in CHO cells that showed stability in PBS buffer after isolation (Gallat et al., 2014). Moreover, putative crystalline inclusions consisting of the nonstructural protein μNS from avian reovirus fused to GFP grew in chicken embryo fibroblasts (CEFs) (Brandariz-Nuñez et al., 2010). A multitude of needle-shaped structures per cell were observed in the cytosol, characterized by comparable dimensions of approximately 1×5 μm. Inside reovirus infected avian cells, μNS is suggested to form the basic scaffold of ordered cytoplasmic inclusions that drive reovirus replication, termed viral factories (Touris-Otero et al., 2004), which might explain the observed self-assembly.

Insect cells

Next to previously mentioned CPV polyhedrin expressed in a heterologous baculovirus system (Coulibaly et al., 2007), crystallization of five entirely different recombinant proteins has been reported in Sf9, Sf21, and High-Five insect cells so far, including: (i) an artificial variant of the heterodimeric phosphatase calcineurin (Figure 2A), forming up to three tetragonal, bipyramidal or cubic shaped crystals in 20–40% of all cells (Fan et al., 1996), (ii) firefly (*Photinus pyralis*) luciferase, forming up to five needle-shaped crystals (Figures 2G and 3) in up to 50% of all cells (Schönherr et al., 2015), (iii) inosine monophosphate dehydrogenase from *T. brucei* (TbIMPDH, Figure 2C), forming several needle-shaped crystals in up to 90% of all cells (Koopmann et al., 2012), (iv) glycosylated cathepsin B from *T. brucei* (TbCatB), forming several needle-shaped crystals (Figure 3) in approximately 70% of all

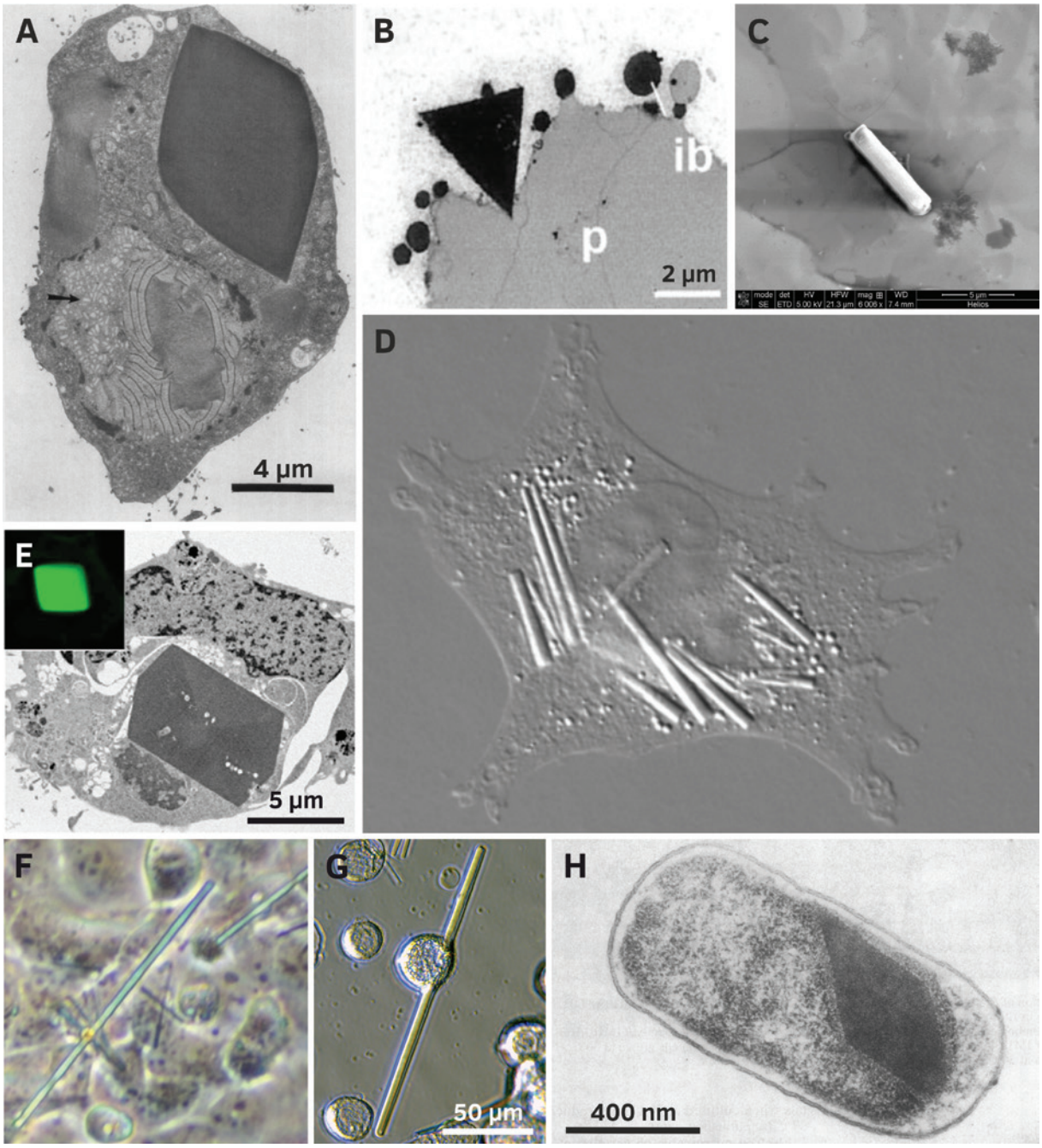

Figure 2: Selected recombinant proteins crystallized in living cells.
(A) Crystal of heterodimeric calcineurin with a human regulatory subunit and a catalytic subunit of *Neurospora crassa* recombinantly produced in *Trichoplusia ni* HighFive cells (Fan et al., 1996; reproduced with permission of John Wiley and Sons). (B) Triangular crystals of pea legumin A developing in outer endosperm cells of transformed wheat (Republished with permission of American Society of Plant Biologists from Stöger et al. (2001); permission conveyed through Copyright Clearance Center, Inc.). (C) Isolated crystal of *Tb*IMPDH produced in Sf9 insect cells (Nass, 2013). (D) Several needle shaped crystals (up to 20 µm in length) of human IgG2 in CHO hamster cells (Hasegawa et al., 2011; © 2011 The American Society for Biochemistry and Molecular Biology). (E) Crystals of Xpa, an engineered coral fluorescent protein, produced in human HEK293 cells (Reprinted from Tsutsui et al. (2015) with permission from Elsevier). (F) Human PAK4cat (the constitutively active catalytic domain) in complex with the PAK4 inhibitor Inka1 co-crystallized in monkey COS-7 cells (Baskaran et al., 2015). (G) A crystal of firefly luciferase (*Photinus pyralis*) in a living Sf9 insect cell. The crystal is about 170 µm long (seven times the cell diameter). (H) Bipyramidal crystal of the 130 kDa toxin from *Bacillus thuringiensis* subsp. *aizawai* IPL7 recombinantly produced in *Escherichia coli* JM103 (Oeda et al., 1989; with permission from American Society for Microbiology).

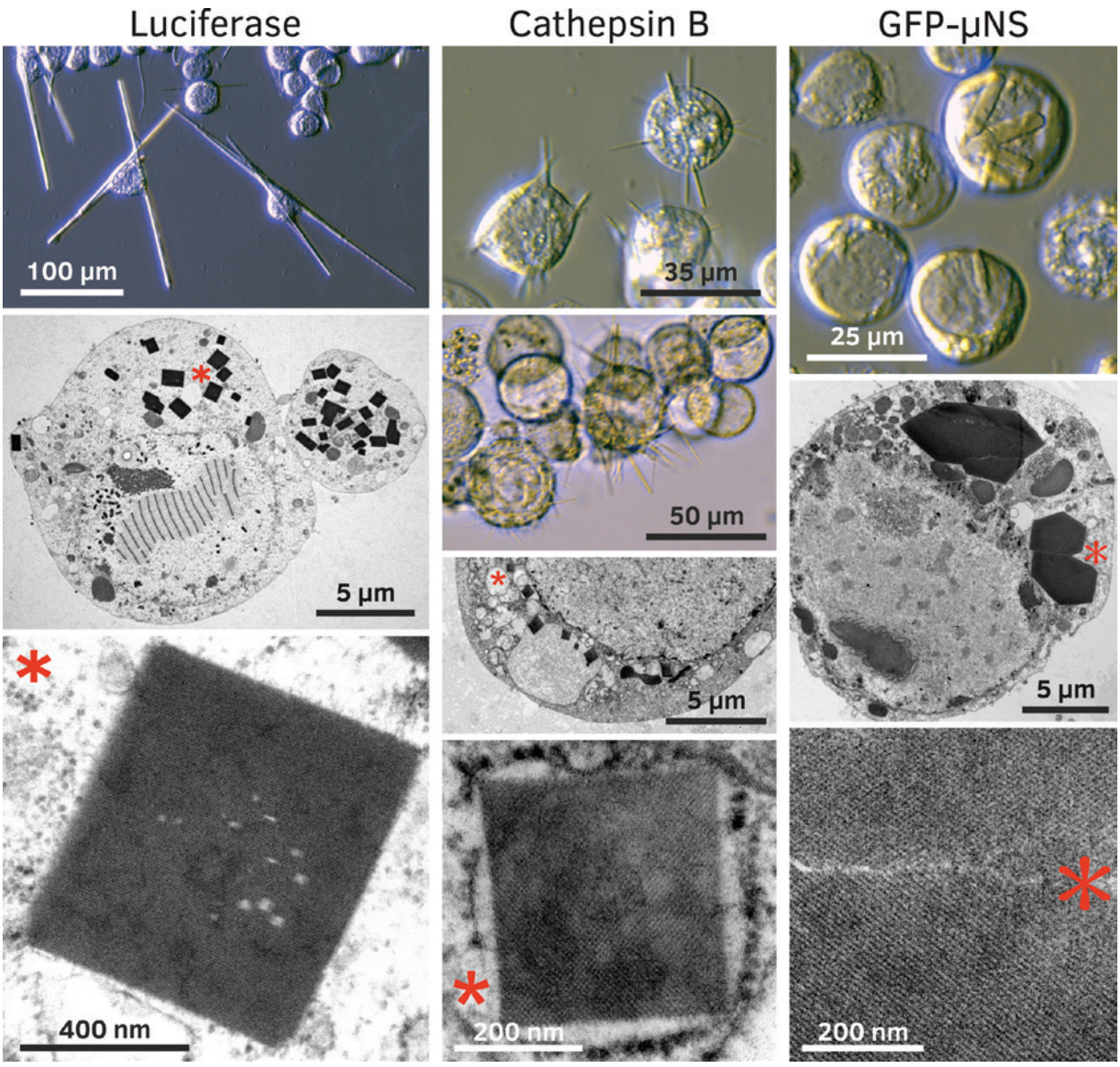

Figure 3: Crystallization of recombinant proteins in insect cells after gene overexpression using the baculovirus insect cell system. Left panel: Crystals of firefly luciferase from *Photinus pyralis* produced in *Trichoplusia ni* HighFive insect cells. Cells can harbor dozens of very long needles, which show a crystalline lattice in TEM studies. Middle panel: Crystals of *Tb*CatB produced in *Trichoplusia ni* HighFive insect cells. Fine needles (0.4–1 μm diameter) do not penetrate through the cellular membranes. Crystals have been used to solve the *Tb*CatB structure (Redecke et al., 2013). Right panel: The reovirus fusion protein GFP-μNS produces needle shaped crystals in *Spodoptera frugiperda* Sf9 insect cells (Schönherr et al., 2015). TEM images show hexagonal structures with a diameter of up to 5 μm and a crystalline lattice. Asterisks in low magnification TEM images denote crystals that have been magnified in the panels below.

cells (Koopmann et al., 2012; Redecke et al., 2013), and (v) the avian reovirus μNS protein linked to GFP (GFP-μNS), forming green fluorescent needles with a hexagonal cross section (Figure 3) in almost all cells of the culture with comparable morphology to the structures detected in CEF cells (Brandariz-Nuñez et al., 2010; Schönherr et al., 2015).

Depending on the native translocation signals harbored in the sequence of the recombinant proteins, crystals occurred in the ER (TbCatB) and in peroxisomes (TbIMPDH, luciferase), next to cytosolic localization (calcineurin, GFP-μNS). For TbIMPDH crystals, an autophagosomal origin of the embedding membrane is additionally

proposed (Duszenko et al., 2015), as observed for Xpa crystals in CHO cells (Tsutsui et al., 2015), but needs to be further investigated. As direct insect cell transfection also results in the growth of comparable luciferase crystals, the baculovirus proteins or the viral replication process itself seems not to be essential for intracellular crystallization, but supports an efficient gene shuttle based on the viral spread (Schönherr et al., 2015).

There is an apparent preference for needle-like structures, but the size of the crystals differs depending on the protein. GFP-μNS and calcineurin assemblies do not extend the regular cell diameter. In contrast, TbCatB, TbIMPDH, and particularly luciferase crystals with an extraordinary length of up to 200 μm clearly protrude out of the living cell, expanding the membrane without affecting cell viability. Remarkably, individual luciferase crystals showed a dynamic degradation and re-assembly within the same living cell over the entire growth period that is unique among *in cellulo* crystals so far, but not understood (Schönherr et al., 2015).

Diffraction of XFEL pulses at TbCatB *in cellulo* crystals allowed determining its high-resolution structure (Redecke et al., 2013), while diffraction tests at least confirmed the crystalline state of TbIMPDH and GFP-μNS assemblies (Koopmann et al., 2012; Schönherr et al., 2015). These experiments exploited the extraordinary mechanical and chemical stability that distinguishes the mentioned crystals after membrane disruption. Luciferase exhibits a significant exception: cell lysis leads to passive crystal dissolution within 3 h even in optimized buffers (Schönherr et al., 2015), preventing diffraction studies so far.

Diffraction data collection using *in cellulo* crystals

Tremendous improvements of X-ray sources and data collection approaches during the past decade paved the way to use even the smallest *in cellulo* crystals with subcellular dimensions as suitable targets for structural investigation (Oberthuer et al., 2017). Today, diverse diffraction data collection strategies are established at state-of-the-art X-ray sources, depending on the demands of the target crystals (Figure 4) (Spence, 2017; Yamamoto et al., 2017). Particularly serial approaches that analyze diffraction of multiple isomorphous microcrystals to overcome conventional radiation dose limits represent successful strategies already applied for *in cellulo* crystals after isolation from the cells or within their native environment (Table 1).

Data collection with isolated crystals

The majority of *in cellulo* crystals used for diffraction data collection so far were isolated and at least partially purified from cells. This strategy was motivated by the extraordinary intrinsic stability of the first diffraction targets, the insect virus polyhedra (Coulibaly et al., 2007), and by the concern that diffuse background scattering of residual cell material might bias the specific crystal diffraction. A multiple crystal synchrotron diffraction approach (MSX) appeared to be highly suitable for crystals with volumes between 1 and 3000 μm^3. The smaller the volume the more isolated crystals usually mounted on MicroMeshes were used to collect interpretable diffraction data at microfocus synchrotron beamlines under cryo conditions. The partial datasets from the different crystals were merged to generate a final dataset with adequate redundancy. This strategy elucidated 16 structures of CPV and baculovirus polyhedra as well as the structure of entomopoxvirus fusolin and of the cockroach milk protein Lili-Mip (Table 1) (Coulibaly et al., 2007, 2009; Ji et al., 2010, 2015; Axford et al., 2014; Chiu et al., 2015; Ginn et al., 2015; Banerjee et al., 2016; Boudes et al., 2016).

If quick deterioration of the diffraction quality due to radiation damage prevents the collection of several high-resolution diffraction patterns from one crystal, serial synchrotron crystallography (SSX) can be applied. Inspired by the SFX strategy, a nylon loop or a MicroMesh loaded with thousands of isolated microcrystals is raster-scanned using a helical line-scan approach. The subset of collected detector frames that contains diffraction signals from individual crystals in random orientations is selected for further processing into a crystallographic data set. SSX was successfully applied to refine a structural model of TbCatB from isolated crystals with an average volume of 9 μm^3 by combination of diffraction data from only 80 crystals (Gati et al., 2014), but resolution was restricted by radiation damage.

The application of SFX at an XFEL outruns resolution limits imposed by crystal size and radiation damage (Spence, 2017). The extremely brilliant and ultra-short X-ray pulses allow room temperature diffraction data collection even from nanometer-sized crystals before destruction by the deposited energy (Chapman et al., 2011). In 2012, the capability of SFX to generate new bioinformation was initially confirmed by elucidation of the native

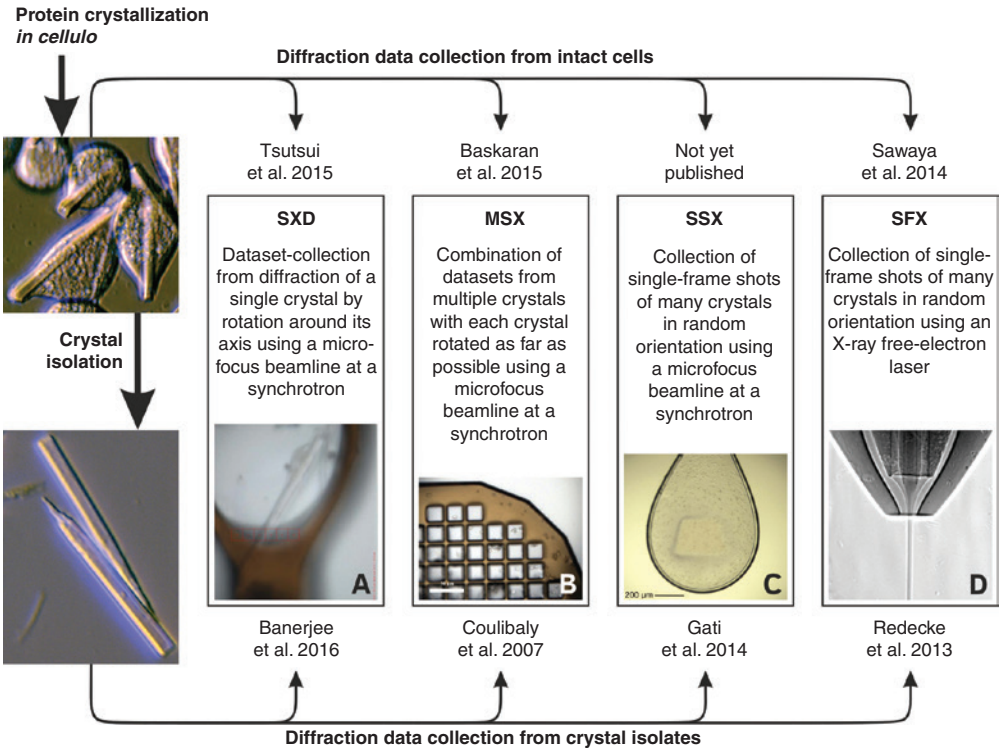

Figure 4: Methods of X-ray diffraction data collection successfully applied on isolated *in cellulo* protein crystals (lower part) or crystals within the intact cells (upper part) and selected publications.
SXD, single-crystal X-ray diffraction applying synchrotron radiation; MSX, multiple-crystal synchrotron crystallography; SSX, serial synchrotron crystallography; SFX, serial femtosecond crystallography; (A) single crystal within a cell mounted in a 200 μm cryogenic loop (Baskaran et al., 2015). (B) Isolated crystals loaded onto a 25 μm MicroMesh (Axford et al., 2014). (C) Suspension of isolated crystals scooped up with a 700 μm cryogenic nylon loop (Gati et al., 2014; reproduced with permission of the International Union of Crystallography). (D) Stream of liquid sample suspension focused by a double flow-focusing nozzle (Oberthuer et al., 2017).

T. brucei pro-cathepsin B structure at 2.1 Å resolution using *in cellulo* crystals (Redecke et al., 2013). Based on this success, the SFX approach was subsequently applied to determine the structure of polyhedrin from CPV type 17 at 1.75 Å (Ginn et al., 2015) and of granulin from *C. pomonella* granulovirus (CpGV) at 2 Å and 2.56 Å (Gati et al., 2017; Oberthuer et al., 2017). Moreover, SFX tests revealed the diffraction capacity of isolated human neuraminidase crystals grown in CHO cells and of cockroach milk protein, without recording of complete datasets (Gallat et al., 2014). Recent improvements in data processing strategies and in sample injection techniques significantly reduced the number of diffraction patterns required to solve a protein structure and sample consumption (Ginn et al., 2015; Oberthuer et al., 2017). A novel sample delivery approach using micropatterned silicon chips in combination with a high-speed goniometer increased crystal hit-rates up to 70% (compared to 1–10% for liquid micro-jets), which in turn dramatically reduced the time required to collect a complete dataset of CPV18 polyhedrin to less than 10 min (Roedig et al., 2017). This highlights the capability of current SFX strategies to collect high-resolution data from smallest *in cellulo* crystals in short time.

In cellulo diffraction data collection

In contrast to the previous examples, firefly luciferase and Xpa crystals grown in insect and mammalian cells, respectively, dissolve quickly after disruption of the cellular membrane (Schönherr et al., 2015; Tsutsui et al., 2015). Thus, subjecting *in cellulo* crystals to tedious isolation and purification procedures might be detrimental. Recently, high quality diffraction data were directly collected within the living cells, denoted as *in cellulo* diffraction, consistently without obscuring specific crystal diffraction by background scattering. Resolution limits of the best diffraction images collected by SFX from toxin crystal-containing *B. thuringiensis* cells were the same as from isolated crystals (Sawaya et al., 2014). This was confirmed

by synchrotron diffraction of CPV polyhedra within insect cells mounted on a MicroMesh at cryo-conditions, clearly disproving previous concerns. Differences between the unit-cell parameters and the mosaic spread together with a gain of 0.35 Å in resolution obtained by *in cellulo* diffraction indicate that even these robust crystals are adversely affected by isolation (Axford et al., 2014; Boudes et al., 2016, 2017). Applying the *in cellulo* diffraction approach, structures of Xpa (Tsutsui et al., 2015) and of the PAK4/Inka-1 complex (Baskaran et al., 2015) were determined from a single crystal at 2.9 Å and from multiple crystals at 2.94 Å, respectively, while single alcohol/methanol oxidase crystals diffracted XFEL pulses up to 6 Å resolution in intact yeast cells (Jakobi et al., 2016). These examples indicate that *in cellulo* diffraction is highly promising to overcome stability problems related to crystal isolation, since the living cell seems to maintain a favorable protective environment for the intracellular crystals. However, a major obstacle that currently limits the determination of entirely new structures from *in cellulo* collected diffraction data is the requirement for experimental phasing. While heavy atom labeling can be achieved by soaking experiments with purified *in cellulo* crystals, as revealed by successful *de novo* structure determination (Coulibaly et al., 2007, 2009; Banerjee et al., 2016; Colletier et al., 2016), intracellular labeling requires selenomethionine substitution within the crystallizing protein or the membrane transfer of heavy metal ions. First indications for a successful metal incorporation were recently reported (Boudes et al., 2016).

Regulation of intracellular protein crystallization

Native *in cellulo* crystallization

Following the basic dogma of X-ray crystallography, all well-folded proteins are assumed to have an intrinsic propensity to readily crystallize, which can probably be accomplished by adjusting the environmental conditions in consideration of the protein's individual biochemical properties (McPherson and Gavira, 2014). Consequently, the crystallization tendency of cellular proteins needs to be tightly regulated to prevent unwanted crystal formation. A balance between protein synthesis and degradation usually maintains local protein concentrations below the solubility limit, rendering nucleation processes thermodynamically unfavorable (Rothman, 2010). If a specific cellular protein should adopt a native crystalline state, its intrinsic crystallization propensity is evolutionary increased, frequently combined with a local concentration by compartmentalization. The former is reflected by readily re-crystallization, reported several-fold for isolated and solubilized native *in cellulo* crystals (Crowfoot and Fankuchen, 1938; Hall, 1950; Yuan et al., 2003; Banerjee et al., 2016). In turn, premature auto-crystallization of the target proteins has to be prevented, which is accomplished by control of intermolecular protein interactions through precursor proteins, specific binding partners, or through environmental changes within the transport pathway towards their destination compartment.

The intrinsic optimization of natively crystallizing proteins that triggers their assembly into crystalline states usually strengthens the intermolecular interactions within the crystal lattice. Several of these proteins exhibit enormous contact interfaces that cover a significant proportion of the protein surface, as observed for BinAB (Colletier et al., 2016), HEX-1 (Yuan et al., 2003), and for insect virus polyhedra (Ji et al., 2015). In the latter example, an improved interface stabilizes a polyhedrin trimer that assembles into a tetrahedral cluster of four trimers, representing the building block of the lattice. The trimers are further cross-linked via molecular 'arms' formed by the protruding helix H1 in CPV polyhedrin or the projecting C-terminal loop in baculoviral polyhedrin, combined with an additional cluster stabilization by intermolecular disulfide bridges (Coulibaly et al., 2007, 2009; Ji et al., 2015). These strong crystal contacts involving the majority of the surface of each trimer are broadly conserved across all known polyhedra, despite many individual differences (Ji et al., 2015). As extended C-terminal molecular arms also interconnect domain-swapped dimers in crystalline fusolin spindles, this cross-linking mechanism has been proposed as a general intrinsic stabilization feature, at least for viral proteins (Chiu et al., 2015). Moreover, the strategy to covalently connect the crystalline matrix by a unique 3D network of disulfide bonds is also observed in fusolin spindles and in *B. thuringiensis* toxins, where the cysteine-rich C-terminal domain of large (135 kDa) protoxins acts as an enhancer of the native crystallization process (Evdokimov et al., 2014). Together with strong salt bridges (Bietlot et al., 1990), the intermolecular disulfide bonds improve the crystallization tendency even in other host cells (De Cosa et al., 2001). For intracellular crystallization of small 3d-Cry protoxins (65 kDa) which lack a C-terminal 'crystallization domain', other factors

are known to be involved, including elements termed 'crystallization'- or 'helper'-proteins, as recently reviewed (Adalat et al., 2017). Regulated crystallization of insulin in secretory granules depends on a specific hexameric state that proinsulin adopts after ribosomal synthesis and ER import only in the presence of zinc ions. However, the proteolytic cleavage of the C peptide during secretory vesicle formation is required to trigger the self-assembly of the hexamers into crystals (Dodson and Steiner, 1998).

Other cellular control mechanisms to prevent premature crystallization are less understood. Baculoviral polyhedrin is suggested to bind importin as an aggregation inhibitor in the cytoplasm prior to transport into the nucleus (Ji et al., 2015). In CPV infected cells the pool concentration of nucleoside triphosphates that are incorporated into the crystal lattice at specific positions might regulate polyhedra assembly (Coulibaly et al., 2007; Ji et al., 2010, 2015). As shown for granulin, the crystalline capsule nucleates either on the end or at the side of the granulosis virus rod and grows until the complete capsule is formed (Arnott and Smith, 1967), but the termination of the crystallization process remains unclear. Envelopes of the viral protein p10, which is also produced in infected cells, are proposed to guide the coating process around the crystals (Van Oers and Vlak, 1997), but further investigation is required.

For several storage- and protection-associated *in cellulo* crystals regulated disassembly is required at highly specific conditions to fulfill their native function. An alkaline pH shift frequently acts as a trigger to distort essential crystal contacts. In viral polyhedra and bacterial BinAB toxin, tyrosine and carboxylate-mediated contacts represent the pH switches. Tyrosine acquires a negative charge after deprotonation that destroys associated hydrogen bonds and leads to repulsion between residues, breaking down the crystal lattice (Coulibaly et al., 2007; Ji et al., 2015; Colletier et al., 2016). If the environment additionally provides reducing conditions, as present in the insect gut, disulfide-based cross-links dissociate, releasing monomeric Cry protoxins for further proteolytic maturation (Soberón et al., 2007). In fusolin spindles, the alkaline pH triggers the removal of the molecular arm by proteolysis, which abolishes the stabilizing network (Chiu et al., 2015), whereas the pH shift from 5.5 to 7.4 during serum release dissolves the insulin crystals into functionally active monomers by disrupting the stabilizing zinc coordination (Dunn, 2005). Moreover, changes in yolk platelet pH during *Xenopus laevis* development correlate with yolk utilization (Fagotto and Maxfield, 1994).

In cellulo crystallization of recombinant proteins

Although the current knowledge is comparatively low, abnormal *in cellulo* crystallization is supposedly affected by other parameters than previously discussed for native crystal growth. If disease-associated mutations increase the intrinsic crystallization tendency of a cellular protein, the cell must regulate the protein level to maintain local concentrations below the nucleation threshold. This could be achieved by activation of degradation pathways or regulation of gene expression on the transcriptional or translational level. In the case of recombinant proteins, regulation of gene expression is usually not an option, leaving the cell with protein degradation as the sole regulatory pathway. However, recombinant expression systems are generally designed for high yield protein production, leading to high local concentrations if the protein is not secreted. This might act as the sole trigger required for crystal nucleation and subsequent growth, if the environmental conditions within the organelle fit.

The theory of concentration-dependent nucleation is supported by a few examples. Best insights into the crystallization process of recombinant proteins were provided by the constitutive high-level production of a human IgG clone in CHO cells engineered by genome integration and gene multiplication (Hasegawa et al., 2011). Based on the cellular phenotype, IgG synthesis and folding might have exceeded the capacity of the ER export machinery, followed by progressive accumulation of well-folded IgG in the ER lumen, until a threshold concentration was reached to nucleate needle-shaped crystals. If the rate of recombinant protein synthesis is reduced, e.g. during transient expression of human IgG in HEK293 cells, inhibition of the cargo export from the ER is required to induce comparable intracellular crystallization (Hasegawa et al., 2011). Consistent results have been obtained after transient expression of other target genes in mammalian and insect cells. Following direct transfection, nucleation of the Xpa protein was only detected in 0.1% of all transfected HEK293 cells (Tsutsui et al., 2015), and a reduced crystallization efficiency was reported after virus-free transfection of Sf9 insect cells with a pIEX4 vector containing the firefly luciferase gene (Schönherr et al., 2015). However, if a recombinant baculovirus is used for gene transfer, gene multiplication that occurs during virus replication within the infected insect cell is supposed to contribute to local protein concentrations, triggering an efficient growth of multiple crystals per cell in a significant fraction of the

cultured cells (Fan et al., 1996; Koopmann et al., 2012; Redecke et al., 2013; Schönherr et al., 2015).

A direct impact of cellular mechanisms on the crystal nucleation process is currently not indicated. In IgG-producing HEK293 cells, all three arms of the unfolded protein response (UPR) were constitutively activated, as expected for cells with a high secretory activity (Hasegawa et al., 2011). This stress response strategy of the ER in higher eukaryotes and yeast is suggested to reduce protein synthesis and to up-regulate protein folding activity (Hetz, 2012), which might fail due to the high protein production rates and the already well-folded recombinant proteins that build the intracellular crystals.

Conclusions

The examples presented in this review clearly reveal that living cells spanning all kingdoms of life occupy the ability to form micrometer-sized intracellular protein crystals that are no longer prevented from structural investigation thanks to the recent revolution in X-ray sources and data collection strategies. Next to cellular proteins that assemble into native crystalline state this also applies to a growing number of recombinant proteins. The abnormal crystallization during heterologous gene expression in host cells under quasi-native conditions eliminates the need for time-consuming optimization of protein purification and for extensive crystal screening steps, additionally preventing distortion that could arise from non-physiological conditions imposed by re-crystallization. Thus, *in cellulo* crystallography might offer exciting new possibilities for proteins that do not form crystals suitable for X-ray diffraction using conventional approaches.

The current knowledge suggests that both the native and abnormal *in cellulo* crystallization depend on a prolific interplay between high local protein concentrations and the intrinsic crystallization tendency of the target protein at the conditions provided by the specific compartment. However, in contrast to heterologous protein assembly, evolutionary optimization of the latter usually triggers native crystallization, which in turn requires a tight control of the intermolecular protein interactions.

A systematic investigation of the intracellular processes involved in crystal formation is required to learn how the crystals grow within cells and what controls their size and shape, but also to identify biological parameters suitable for screening approaches, opening *in cellulo* crystallization into a widely applicable field.

An initial setup of a pipeline that further exploits the crystallization capability of living insect cells, followed by flow cytometry sorting and direct analysis of the crystals by *in cellulo* X-ray diffraction, was already proposed and recently applied to recombinant CPV1 polyhedrin crystals (Boudes et al., 2016, 2017). Furthermore, the specific lattice features of some *in cellulo* crystals were proposed to facilitate the crystallization of recombinant fusion proteins by acting as an array in which guest molecules can reside for X-ray analysis (Mori et al., 2010; Baskaran et al., 2015). While it is yet unknown how widely applicable *in cellulo* crystallization may be, it is clear from the examples discussed here that there is a reason to be optimistic that it can be achieved in many cases.

Acknowledgments: J.M.R. acknowledges funding through a PhD scholarship of the Joachim Herz Stiftung, Funder Id: 10.13039/100008662 "PhD scholarship". R.S. and L.R. are grateful for support from the DFG, Funder Id: 10.13039/501100001659, Cluster of Excellence "Inflammation at Interfaces" (EXC 306).

References

Ackerman, S.J., Liu, L., Kwatia, M.A., Savage, M.P., Leonidas, D.D., Swaminathan, G.J., and Acharya, K.R. (2002). Charcot-Leyden crystal protein (galectin-10) is not a dual function galectin with lysophospholipase activity but binds a lysophospholipase inhibitor in a novel structural fashion. J. Biol. Chem. *277*, 14859–14868.

Adalat, R., Saleem, F., Crickmore, N., Naz, S., and Shakoori, A.R. (2017). *In vivo* crystallization of three-domain Cry toxins. Toxins *9*, 80.

Albers, S.-V. and Meyer, B.H. (2011). The archaeal cell envelope. Nat. Rev. Microbiol. *9*, 414–426.

Anduleit, K., Sutton, G., Diprose, J.M., Mertens, P.P.C., Grimes, J.M., and Stuart, D.I. (2005). Crystal lattice as biological phenotype for insect viruses. Protein Sci. *14*, 2741–2743.

Arnott, H.J. and Smith, K.M. (1967). An ultrastructural study of the development of a granulosis virus in the cells of the moth *Plodia interpunctella* (Hbn.). J. Ultrastruct. Res. *21*, 251–268.

Arvan, P. and Castle, D. (1998). Sorting and storage during secretory granule biogenesis: looking backward and looking forward. Biochem. J. *332*, 593–610.

Axford, D., Ji, X., Stuart, D.I., and Sutton, G. (2014). *In cellulo* structure determination of a novel cypovirus polyhedrin. Acta Crystallogr. D Biol. Crystallogr. *70*, 1435–1441.

Banerjee, S., Coussens, N.P., Gallat, F.-X., Sathyanarayanan, N., Srikanth, J., Yagi, K.J., Gray, J.S.S., Tobe, S.S., Stay, B., Chavas, L.M.G., et al. (2016). Structure of a heterogeneous, glycosylated, lipid-bound, in vivo-grown protein crystal at atomic resolution from the viviparous cockroach *Diploptera punctata*. IUCrJ *3*, 282–293.

Baskaran, Y., Ang, K.C., Anekal, P. V., Chan, W.L., Grimes, J.M., Manser, E., and Robinson, R.C. (2015). An *in cellulo*-derived structure of PAK4 in complex with its inhibitor Inka1. Nat. Commun. *6*, 8681.

Bietlot, H.P., Vishnubhatla, I., Carey, P.R., Pozsgay, M., and Kaplan, H. (1990). Characterization of the cysteine residues and disulphide linkages in the protein crystal of *Bacillus thuringiensis*. Biochem. J. *267*, 309–315.

Bill, R.M., Henderson, P.J.F., Iwata, S., Kunji, E.R.S., Michel, H., Neutze, R., Newstead, S., Poolman, B., Tate, C.G., and Vogel, H. (2011). Overcoming barriers to membrane protein structure determination. Nat. Biotechnol. *29*, 335–340.

Boudes, M., Garriga, D., Fryga, A., Caradoc-Davies, T., and Coulibaly, F. (2016). A pipeline for structure determination of *in vivo*-grown crystals using in cellulo diffraction. Acta Crystallogr. D Struct. Biol. *72*, 576–585.

Boudes, M., Garriga, D., and Coulibaly, F. (2017). Microcrystallography of protein crystals and *in cellulo* diffraction. J. Vis. Exp. *21*, e55793.

Brandariz-Nuñez, A., Menaya-Vargas, R., Benavente, J., and Martinez-Costas, J. (2010). Avian reovirus microNS protein forms homo-oligomeric inclusions in a microtubule-independent fashion, which involves specific regions of its C-terminal domain. J. Virol. *84*, 4289–4301.

Chapman, H.N., Fromme, P., Barty, A., White, T.A., Kirian, R.A., Aquila, A., Hunter, M.S., Schulz, J., DePonte, D.P., Weierstall, U., et al. (2011). Femtosecond X-ray protein nanocrystallography. Nature *470*, 73–77.

Charcot, J.M. and Robin, C. (1853). Observation of leukocytosis. CR Mem. Soc. Biol. *5*, 450–454.

Chayen, N.E. and Saridakis, E. (2008). Protein crystallization: from purified protein to diffraction-quality crystal. Nat. Methods *5*, 147–153.

Chen, Q., Vekilov, P.G., Nagel, R.L., and Hirsch, R.E. (2004). Liquid-liquid phase separation in hemoglobins: distinct aggregation mechanisms of the β6 mutants. Biophys. J. *86*, 1702–1712.

Chiu, E., Hijnen, M., Bunker, R.D., Boudes, M., Rajendran, C., Aizel, K., Oliéric, V., Schulze-Briese, C., Mitsuhashi, W., Young, V., et al. (2015). Structural basis for the enhancement of virulence by viral spindles and their *in vivo* crystallization. Proc. Natl. Acad. Sci. USA *112*, 3973–3978.

Colletier, J.-P., Sawaya, M.R., Gingery, M., Rodriguez, J.A., Cascio, D., Brewster, A.S., Michels-Clark, T., Hice, R.H., Coquelle, N., Boutet, S., et al. (2016). *De novo* phasing with X-ray laser reveals mosquito larvicide BinAB structure. Nature *539*, 43–47.

Colman, P.M., Suzuki, E., and Van Donkelaar, A. (1980). The structure of cucurbitin: subunit symmetry and organization *in situ*. Eur. J. Biochem. *103*, 585–588.

Coulibaly, F., Chiu, E., Ikeda, K., Gutmann, S., Haebel, P.W., Schulze-Briese, C., Mori, H., and Metcalf, P. (2007). The molecular organization of cypovirus polyhedra. Nature *446*, 97–101.

Coulibaly, F., Chiu, E., Gutmann, S., Rajendran, C., Haebel, P.W., Ikeda, K., Mori, H., Ward, V.K., Schulze-Briese, C., and Metcalf, P. (2009). The atomic structure of baculovirus polyhedra reveals the independent emergence of infectious crystals in DNA and RNA viruses. Proc. Natl. Acad. Sci. USA *106*, 22205–22210.

Crowfoot, D. and Fankuchen, I. (1938). Molecular weight of a tobacco seed globulin. Nature *141*, 522–523.

De Cosa, B., Moar, W., Lee, S.-B., Miller, M., and Daniell, H. (2001). Overexpression of the Bt cry2Aa2 operon in chloroplasts leads to formation of insecticidal crystals. Nat. Biotechnol. *19*, 71–74.

Dodson, G. and Steiner, D. (1998). The role of assembly in insulin's biosynthesis. Curr. Opin. Struct. Biol. *8*, 189–194.

Dogan, S., Barnes, L., and Cruz-Vetrano, W.P. (2012). Crystal-storing histiocytosis: report of a case, review of the literature (80 cases) and a proposed classification. Head Neck Pathol. *6*, 111–120.

Doye, J.P.K. and Poon, W.C.K. (2006). Protein crystallization *in vivo*. Curr. Opin. Colloid Interface Sci. *11*, 40–46.

Doye, J.P.K., Louis, A.A., and Vendruscolo, M. (2004). Inhibition of protein crystallization by evolutionary negative design. Phys. Biol. *1*, P9–13.

Dunn, M.F. (2005). Zinc-ligand interactions modulate assembly and stability of the insulin hexamer – a review. BioMetals *18*, 295–303.

Duszenko, M., Redecke, L., Mudogo, C.N., Sommer, B.P., Mogk, S., Oberthuer, D., and Betzel, C. (2015). *In vivo* protein crystallization in combination with highly brilliant radiation sources offers novel opportunities for the structural analysis of post-translationally modified eukaryotic proteins. Acta Crystallogr. F Struct. Biol. Commun. *71*, 929–937.

Duyvesteyn, H.M.E., Ginn, H.M., Pietilä, M.K., Wagner, A., Hattne, J., Grimes, J.M., Hirvonen, E., Evans, G., Parsy, M.-L., Sauter, N.K., et al. (2018). Towards *in cellulo* virus crystallography. Sci. Rep. *8*, 3771.

Evdokimov, A.G., Moshiri, F., Sturman, E.J., Rydel, T.J., Zheng, M., Seale, J.W., and Franklin, S. (2014). Structure of the full-length insecticidal protein Cry1Ac reveals intriguing details of toxin packaging into *in vivo* formed crystals. Protein Sci. *23*, 1491–1497.

Fagotto, F. and Maxfield, F.R. (1994). Changes in yolk platelet pH during *Xenopus laevis* development correlate with yolk utilization. A quantitative confocal microscopy study. J. Cell Sci. *107*, 3325–3337.

Fan, G.Y., Maldonado, F., Zhang, Y., Kincaid, R., Ellisman, M.H., and Gastinel, L.N. (1996). *In vivo* calcineurin crystals formed using the baculovirus expression system. Microsc. Res. Tech. *34*, 77–86.

Farrants, G.W., Fil, S.H., and Stadhouders, A.M. (1988). Two types of mitochondrial crystals in diseased human skeletal muscle fibers. Muscle Nerve *11*, 45–55.

Feeling-Taylor, A.R., Yau, S.-T., Petsev, D.N., Nagel, R.L., Hirsch, R.E., and Vekilov, P.G. (2004). Crystallization mechanisms of hemoglobin C in the R state. Biophys. J. *87*, 2621–2629.

Freddo, T.F., Townes-Anderson, E., and Raviola, G. (1980). Rod-shaped bodies and crystalloid inclusions in ocular vascular endothelia of adult and developing *Macaca mulatta*. Anat. Embryol. *158*, 121–131.

Frigas, E. and Gleich, G.J. (1986). The eosinophil and the pathophysiology of asthma. J. Allergy Clin. Immunol. *77*, 527–537.

Gallat, F.-X., Matsugaki, N., Coussens, N.P., Yagi, K.J., Boudes, M., Higashi, T., Tsuji, D., Tatano, Y., Suzuki, M., Mizohata, E., et al. (2014). *In vivo* crystallography at X-ray free-electron lasers: the next generation of structural biology? Phil. Trans. R. Soc. B *369*, 20130497.

Gati, C., Bourenkov, G., Klinge, M., Rehders, D., Stellato, F., Oberthür, D., Yefanov, O., Sommer, B.P., Mogk, S., Duszenko, M., et al. (2014). Serial crystallography on *in vivo* grown microcrystals using synchrotron radiation. IUCrJ *1*, 87–94.

Gati, C., Oberthuer, D., Yefanov, O., Bunker, R.D., Stellato, F., Chiu, E., Yeh, S.-M., Aquila, A., Basu, S., Bean, R., et al. (2017). Atomic structure of granulin determined from native nanocrystalline granulovirus using an X-ray free-electron laser. Proc. Natl. Acad. Sci. USA *114*, 2247–2252.

Giembycz, M. and Lindsay, M. (1999). Pharmacology of the eosinophil. Pharmacol. Rev. *51*, 213–340.

Ginn, H.M., Messerschmidt, M., Ji, X., Zhang, H., Axford, D., Gildea, R.J., Winter, G., Brewster, A.S., Hattne, J., Wagner, A., et al. (2015). Structure of CPV17 polyhedrin determined by the improved analysis of serial femtosecond crystallographic data. Nat. Commun. *6*, 6435.

Hall, C.E. (1950). Electron microscopy of crystalline edestin. J. Biol. Chem. *185*, 45–51.

Hammersen, F., Gidlöf, A., Larsson, J., and Lewis, D.H. (1980). The occurrence of paracrystalline mitochondrial inclusions in normal human skeletal muscle. Acta Neuropathol. *49*, 35–41.

Hartig, T. (1855). About the gluten flour. Bot. Zeitung *13*, 881–882.

Hasegawa, H., Wendling, J., He, F., Trilisky, E., Stevenson, R., Franey, H., Kinderman, F., Li, G., Piedmonte, D.M., Osslund, T., et al. (2011). *In vivo* crystallization of human IgG in the endoplasmic reticulum of engineered chinese hamster ovary (CHO) cells. J. Biol. Chem. *286*, 19917–19931.

Hasegawa, H., Forte, C., Barber, I., Turnbaugh, S., Stoops, J., Shen, M., and Lim, A.C. (2014). Modulation of *in vivo* IgG crystallization in the secretory pathway by heavy chain isotype class switching and N-linked glycosylation. Biochim. Biophys. Acta *1843*, 1325–1338.

Hawkes, F. (1993). Presence of a crystal in the cytoplasm of the male germ cells of the garden dormouse *Eliomys quercinus* L. J. Submicrosc. Cytol. Pathol. *25*, 407–415.

Heinze, M., Reichelt, R., Kleff, S., and Eising, R. (2000). High resolution scanning electron microscopy of protein inclusions (cores) purified from peroxisomes of sunflower (*Helianthus annuus* L.) Cotyledons. Cryst. Res. Technol. *35*, 877–886.

Hejtmancik, J.F., Kaiser, M.I., and Piatigorsky, J. (1995). Molecular biology and inherited disorders of the eye lens. In: The Metabolic and Molecular Bases of Inherited Disease, C.R. Scriver, A.L. Beaudet, W.S. Sly, and D. Valle, eds. (New York, USA: McGraw-Hill), pp. 4325–4349.

Héon, E., Priston, M., Schorderet, D.F., Billingsley, G.D., Girard, P.O., Lubsen, N., and Munier, F.L. (1999). The γ-crystallins and human cataracts: a puzzle made clearer. Am. J. Hum. Genet. *65*, 1261–1267.

Hetz, C. (2012). The unfolded protein response: controlling cell fate decisions under ER stress and beyond. Nat. Rev. Mol. Cell Biol. *13*, 89–102.

Hill, C.L., Booth, T.F., Stuart, D.I., and Mertens, P.P. (1999). Lipofectin increases the specific activity of cypovirus particles for cultured insect cells. J. Virol. Methods *78*, 177–189.

Holton, J.M. and Frankel, K.A. (2010). The minimum crystal size needed for a complete diffraction data set. Acta Crystallogr. D Biol. Crystallogr. *66*, 393–408.

Hurko, O., Johns, D.R., Rutledge, S.L., Stine, O.C., Peterson, P.L., Miller, N.R., Martens, M.E., Drachman, D.B., Brown, R.H., and Lee, C.P. (1990). Heteroplasmy in chronic external ophthalmoplegia: clinical and molecular observations. Pediatr. Res. *28*, 542–548.

Ingram, M.J., Stay, B., and Cain, G.D. (1977). Composition of milk from the viviparous cockroach, *Diploptera punctata*. Insect Biochem. *7*, 257–267.

Jain, M., Aiyer, H.M., Bajaj, P., and Dhar, S. (2001). Intracytoplasmic and intranuclear Reinke's crystals in a testicular Leydig-cell tumor diagnosed by fine-needle aspiration cytology: a case report with review of the literature. Diagn. Cytopathol. *25*, 162–164.

Jakobi, A.J., Passon, D.M., Knoops, K., Stellato, F., Liang, M., White, T.A., Seine, T., Messerschmidt, M., Chapman, H.N., and Wilmanns, M. (2016). *In cellulo* serial crystallography of alcohol oxidase crystals inside yeast cells. IUCrJ *3*, 88–95.

Ji, X., Sutton, G., Evans, G., Axford, D., Owen, R., and Stuart, D.I. (2010). How baculovirus polyhedra fit square pegs into round holes to robustly package viruses. EMBO J. *29*, 505–514.

Ji, X., Axford, D., Owen, R., Evans, G., Ginn, H.M., Sutton, G., and Stuart, D.I. (2015). Polyhedra structures and the evolution of the insect viruses. J. Struct. Biol. *192*, 88–99.

Jiang, L., Phillips, T.E., Rogers, S.W., and Rogers, J.C. (2000). Biogenesis of the protein storage vacuole crystalloid. J. Cell Biol. *150*, 755–770.

Karas, V.O., Westerlaken, I., and Meyer, A.S. (2015). The DNA-binding protein from starved cells (Dps) utilizes dual functions to defend cells against multiple stresses. J. Bacteriol. *197*, 3206–3215.

Ke, Z., Strauss, J.D., Hampton, C.M., Brindley, M.A., Dillard, R.S., Leon, F., Lamb, K.M., Plemper, R.K., and Wright, E.R. (2018). Promotion of virus assembly and organization by the measles virus matrix protein. Nat. Commun. *9*, 1736.

Kerfeld, C.A. and Erbilgin, O. (2015). Bacterial microcompartments and the modular construction of microbial metabolism. Trends Microbiol. *23*, 22–34.

Knoblauch, M., Peters, W.S., Ehlers, K., and van Bel, A.J. (2001). Reversible calcium-regulated stopcocks in legume sieve tubes. Plant Cell *13*, 1221–1230.

Koopmann, R., Cupelli, K., Redecke, L., Nass, K., DePonte, D.P., White, T.A., Stellato, F., Rehders, D., Liang, M., Andreasson, J., et al. (2012). *In vivo* protein crystallization opens new routes in structural biology. Nat. Methods *9*, 259–262.

Kozina, V., Geist, D., Kubinová, L., Bilić, E., Karnthaler, H.P., Waitz, T., Janáček, J., Chernyavskiy, O., Krhen, I., and Ježek, D. (2011). Visualization of Reinke's crystals in normal and cryptorchid testis. Histochem. Cell Biol. *135*, 215–228.

Lange, R.H., Grodziński, Z., and Kilarski, W. (1982). Yolk-platelet crystals in three ancient bony fishes: *Polypterus bichir* (Polypteri), *Amia calva* L., and *Lepisosteus osseus* (L.) (Holostei). Cell Tissue Res. *222*, 159–165.

Lawrence, C., Fabry, M.E., and Nagel, R.L. (1991). The unique red cell heterogeneity of SC disease: crystal formation, dense reticulocytes, and unusual morphology. Blood *78*, 2104–2112.

Lewis, J.T., Candelora, J.N., Hogan, R.B., Briggs, F.R., and Abraham, S.C. (2007). Crystal-storing histiocytosis due to massive accumulation of Charcot-Leyden crystals: a unique association producing colonic polyposis in a 78-year-old woman with eosinophilic colitis. Am. J. Surg. Pathol. *31*, 481–485.

Leyden, E. (1872). Zur Kenntnis des Bronchial-Asthma. Arch. für Pathol. Anat. und Physiol. und für Klin. Medizin *54*, 324–352.

Luijsterburg, M.S., Noom, M.C., Wuite, G.J.L., and Dame, R.T. (2006). The architectural role of nucleoid-associated proteins in the organization of bacterial chromatin: a molecular perspective. J. Struct. Biol. *156*, 262–272.

Markham, P. and Collinge, A.J. (1987). Woronin bodies of filamentous fungi. FEMS Microbiol. Lett. *46*, 1–11.

Massover, W.H. (1971). Intramitochondrial yolk-crystals of frog oocytes. I. Formation of yolk-crystal inclusions by mitochondria during bullfrog oogenesis. J. Cell Biol. *48*, 266–279.

McPherson, A. and Gavira, J.A. (2014). Introduction to protein crystallization. Acta Crystallogr. F. Struct. Biol. Commun. *70*, 2–20.

Mori, H., Ijiri, H., and Kotani, E. (2010). Application of insect virus polyhedra to protein nanocontainers. Tech. Proc. 2010 NSTI Nanotechnol. Conf. Expo *3*, 254–257.

Nagel, R.L. and Lawrence, C. (1991). The distinct pathobiology of sickle cell-hemoglobin C disease. Therapeutic implications. Hematol. Oncol. Clin. North Am. *5*, 433–451.

Nass, K.J. (2013). Investigation of protein structure determination using X-ray free-electron lasers. PhD thesis, University of Hamburg, Hamburg, Germany.

Nürnberger, S., Rentenberger, C., Thiel, K., Schädl, B., Grunwald, I., Ponomarev, I., Marlovits, S., Meyer, C., and Barnewitz, D. (2017). Giant crystals inside mitochondria of equine chondrocytes. Histochem. Cell Biol. *147*, 635–649.

Oberthuer, D., Knoška, J., Wiedorn, M.O., Beyerlein, K.R., Bushnell, D.A., Kovaleva, E.G., Heymann, M., Gumprecht, L., Kirian, R.A., Barty, A., et al. (2017). Double-flow focused liquid injector for efficient serial femtosecond crystallography. Sci. Rep. *7*, 44628.

Oeda, K., Inouye, K., Ibuchi, Y., Oshie, K., Shimizu, M., Nakamura, K., Nishioka, R., Takada, Y., and Ohkawa, H. (1989). Formation of crystals of the insecticidal proteins of Bacillus thuringiensis subsp. aizawai IPL7 in *Escherichia coli*. J. Bacteriol. *171*, 3568–3571.

Pande, A., Pande, J., Asherie, N., Lomakin, A., Ogun, O., King, J., and Benedek, G.B. (2001). Crystal cataracts: human genetic cataract caused by protein crystallization. Proc. Natl. Acad. Sci. USA *98*, 6116–6120.

Papassideri, I.S., Trougakos, I.P., Leonard, K.R., and Margaritis, L.H. (2007). Crystalline yolk spheroids in *Drosophila melanogaster* oocyte: freeze fracture and two-dimensional reconstruction analysis. J. Insect Physiol. *53*, 370–376.

Payne, C.C. and Mertens, P.P.C. (1983). The cytoplasmic polyhedrosis viruses (New York, USA: Plenum Press).

Perera, S., Li, Z., Pavlik, L., and Arif, B. (2010). Insect Virology (Norwich, UK: Caister Academic).

Plegaria, J.S. and Kerfeld, C.A. (2017). Engineering nanoreactors using bacterial microcompartment architectures. Curr. Opin. Biotechnol. *51*, 1–7.

Raška, I., Komrska, J., Titlbach, M., and Rieder, M. (1978). Fine structure of crystalline inclusions in B-cells of the islets of Langerhans in the alligator. Cell Tissue Res. *187*, 535–550.

Redecke, L., Nass, K., DePonte, D.P., White, T.A., Rehders, D., Barty, A., Stellato, F., Liang, M., Barends, T.R.M., Boutet, S., et al. (2013). Natively inhibited *Trypanosoma brucei* cathepsin B structure determined by using an X-ray laser. Science *339*, 227–230.

Reinke, F. (1896). Contributions to the human histology. I. About the formation of crystalloids in interstitial cells of the human testis. Arch. für Mikroskopische Anat. *47*, 34–44.

Roedig, P., Ginn, H.M., Pakendorf, T., Sutton, G., Harlos, K., Walter, T.S., Meyer, J., Fischer, P., Duman, R., Vartiainen, I., et al. (2017). High-speed fixed-target serial virus crystallography. Nat. Methods *14*, 805–810.

Rohrmann, G.F. (1986). Polyhedrin structure. J. Gen. Virol. *67*, 1499–1513.

Rothman, S. (2010). How is the balance between protein synthesis and degradation achieved? Theor. Biol. Med. Model. *7*, 1–11.

Sanahuja, G., Banakar, R., Twyman, R.M., Capell, T., and Christou, P. (2011). *Bacillus thuringiensis*: a century of research, development and commercial applications. Plant Biotechnol. J. *9*, 283–300.

Sára, M. and Sleytr, U.B. (2000). S-Layer proteins. J. Bacteriol. *182*, 859–868.

Sawaya, M.R., Cascio, D., Gingery, M., Rodriguez, J., Goldschmidt, L., Colletier, J.-P., Messerschmidt, M.M., Boutet, S., Koglin, J.E., Williams, G.J., et al. (2014). Protein crystal structure obtained at 2.9 Å resolution from injecting bacterial cells into an X-ray free-electron laser beam. Proc. Natl. Acad. Sci. USA *111*, 12769–12774.

Schnepf, E., Crickmore, N., Van Rie, J., Lereclus, D., Baum, J., Feitelson, J., Zeigler, D.R., and Dean, D.H. (1998). *Bacillus thuringiensis* and its pesticidal crystal proteins. Microbiol. Mol. Biol. Rev. *62*, 775–806.

Schönherr, R., Klinge, M., Rudolph, J.M., Fita, K., Rehders, D., Lübber, F., Schneegans, S., Majoul, I.V., Duszenko, M., Betzel, C., et al. (2015). Real-time investigation of dynamic protein crystallization in living cells. Struct. Dyn. *2*, 41712.

Shively, J.M., Ball, F.L., and Kline, B.W. (1973). Electron microscopy of the carboxysomes (polyhedral bodies) of *Thiobacillus neapolitanus*. J. Bacteriol. *116*, 1405–1411.

Sleytr, U.B., Schuster, B., Egelseer, E.-M., and Pum, D. (2014). S-layers: principles and applications. FEMS Microbiol. Rev. *38*, 823–864.

Smeitink, J., Stadhouders, A., Sengers, R., Ruitenbeek, W., Wevers, R., ter Laak, H., and Trijbels, F. (1992). Mitochondrial creatine kinase containing crystals, creatine content and mitochondrial creatine kinase activity in chronic progressive external ophthalmoplegia. Neuromuscul. Disord. *2*, 35–40.

Smith, K.M. (1976). Virus-Insect Relationships (London, UK: Longman).

Snigirevskaya, E.S., Hays, A.R., and Raikhel, A.S. (1997). Secretory and internalization pathways of mosquito yolk protein precursors. Cell Tissue Res. *290*, 129–142.

Soberón, M., Fernández, L.E., Pérez, C., Gill, S.S., and Bravo, A. (2007). Mode of action of mosquitocidal *Bacillus thuringiensis* toxins. Toxicon *49*, 597–600.

Soragni, A., Yousefi, S., Stoeckle, C., Soriaga, A.B., Sawaya, M.R., Kozlowski, E., Schmid, I., Radonjic-Hoesli, S., Boutet, S., Williams, G.J., et al. (2015). Toxicity of eosinophil MBP is repressed by intracellular crystallization and promoted by extracellular aggregation. Mol. Cell *57*, 1011–1021.

Spence, J.C.H. (2017). XFELs for structure and dynamics in biology. IUCrJ *4*, 322–339.

Stöger, E., Parker, M., Christou, P., and Casey, R. (2001). Pea legumin overexpressed in wheat endosperm assembles into an ordered paracrystalline matrix. Plant Physiol. *125*, 1732–1742.

Strunk, S.W. (1959). The formation of intracellular crystals in midgut glands of *Limnoria lignorum*. J. Biophys. Biochem. Cytol. *5*, 385–392.

Takemoto, Y., Mitsuhashi, W., Murakami, R., Konishi, H., and Miyamoto, K. (2008). The N-terminal region of an entomopoxvirus fusolin is essential for the enhancement of peroral infection, whereas the C-terminal region is eliminated in digestive juice. J. Virol. *82*, 12406–12415.

Tenney, K., Hunt, I., Sweigard, J., Pounder, J.I., McClain, C., Bowman, E.J., and Bowman, B.J. (2000). *hex-1*, a gene unique to filamentous fungi, encodes the major protein of the Woronin body and functions as a plug for septal pores. Fungal Genet. Biol. *31*, 205–217.

Touris-Otero, F., Martínez-Costas, J., Vakharia, V.N., and Benavente, J. (2004). Avian reovirus nonstructural protein μNS forms viroplasm-like inclusions and recruits protein σNS to these structures. Virology *319*, 94–106.

Tsukada, H., Mochizuki, Y., and Fujiwara, S. (1966). The nucleoids of rat liver cell microbodies. Fine structure and enzymes. J. Cell Biol. *28*, 449–460.

Tsutsui, H., Jinno, Y., Shoda, K., Tomita, A., Matsuda, M., Yamashita, E., Katayama, H., Nakagawa, A., and Miyawaki, A. (2015). A diffraction-quality protein crystal processed as an autophagic cargo. Mol. Cell *58*, 186–193.

Turkewitz, A.P. (2004). Out with a bang! Tetrahymena as a model system to study secretory granule biogenesis. Traffic *5*, 63–68.

van Bel, A.J.E. (2003). The phloem, a miracle of ingenuity. Plant Cell Environ. *26*, 125–149.

Van Oers, M.M. and Vlak, J.M. (1997). The baculovirus 10-kDa protein. J. Invertebr. Pathol. *70*, 1–17.

Vayssié, L., Skouri, F., Sperling, L., and Cohen, J. (2000). Molecular genetics of regulated secretion in paramecium. Biochimie *82*, 269–288.

Veenhuis, M., van Dijken, J.P., Pilon, S.A., and Harder, W. (1978). Development of crystalline peroxisomes in methanol-grown cells of the yeast *Hansenula polymorpha* and its relation to environmental conditions. Arch. Microbiol. *117*, 153–163.

Veenhuis, M., Harder, W., van Dijken, J.P., and Mayer, F. (1981). Substructure of crystalline peroxisomes in methanol-grown *Hansenula polymorpha*: evidence for an *in vivo* crystal of alcohol oxidase. Mol. Cell. Biol. *1*, 949–957.

Veenhuis, M., Kiel, J.A.K.W., and Van der Klei, I.J. (2003). Peroxisome assembly in yeast. Microsc. Res. Tech. *61*, 139–150.

Vekilov, P.G., Feeling-Taylor, A.R., Petsev, D.N., Galkin, O., Nagel, R.L., and Hirsch, R.E. (2002). Intermolecular interactions, nucleation, and thermodynamics of crystallization of hemoglobin C. Biophys. J. *83*, 1147–1156.

Vonck, J. and van Bruggen, E.F. (1992). Architecture of peroxisomal alcohol oxidase crystals from the methylotrophic yeast *Hansenula polymorpha* as deduced by electron microscopy. J. Bacteriol. *174*, 5391–5399.

Ward, R.T. (1962). The origin of protein and fatty yolk in *Rana pipiens*. II. Electron microscopical and cytochemical observations of young and mature oocytes. J. Cell Biol. *14*, 309–341.

Weller, P.F., Bach, D.S., and Austen, F.K. (1984). Biochemical characterization of human eosinophil Charcot-Leyden crystal protein (lysophospholipase). J. Biol. Chem. *259*, 15100–15105.

Williford, A., Stay, B., and Bhattacharya, D. (2004). Evolution of a novel function: nutritive milk in the viviparous cockroach, *Diploptera punctata*. Evol. Dev. *6*, 67–77.

Wolf, S.G., Frenkiel, D., Arad, T., Finkel, S.E., Kolter, R., and Minsky, A. (1999). DNA protection by stress-induced biocrystallization. Nature *400*, 83–85.

Würtz, C., Schliebs, W., Erdmann, R., and Rottensteiner, H. (2008). Dynamin-like protein-dependent formation of Woronin bodies in *Saccharomyces cerevisiae* upon heterologous expression of a single protein. FEBS J. *275*, 2932–2941.

Yabashi, M. and Tanaka, H. (2017). The next ten years of X-ray science. Nat. Photonics *11*, 12–14.

Yamamoto, M., Hirata, K., Yamashita, K., Hasegawa, K., Ueno, G., Ago, H., and Kumasaka, T. (2017). Protein microcrystallography using synchrotron radiation. IUCrJ *4*, 529–539.

Yuan, P., Jedd, G., Kumaran, D., Swaminathan, S., Shio, H., Hewitt, D., Chua, N.-H., and Swaminathan, K. (2003). A HEX-1 crystal lattice required for Woronin body function in *Neurospora crassa*. Nat. Struct. Biol. *10*, 264–270.